Review

N-Doped Graphene and Its Derivatives as Resistive Gas Sensors: An Overview

Ali Mirzaei [1] , **Somalapura Prakasha Bharath** [2] , **Jin-Young Kim** [3] , **Krishna K. Pawar** [2,3] , **Hyoun Woo Kim** [2,4,*] and **Sang Sub Kim** [3,*]

1   Department of Materials Science and Engineering, Shiraz University of Technology, Shiraz 71557-13876, Iran; mirzaei@sutech.ac.ir
2   Division of Materials Science and Engineering, Hanyang University, Seoul 04763, Republic of Korea; pbharathbhat@gmail.com (S.P.B.); 1krishnaisk@gmail.com (K.K.P.)
3   Department of Materials Science and Engineering, Inha University, Incheon 22212, Republic of Korea; piadote@naver.com
4   The Research Institute of Industrial Science, Hanyang University, Seoul 04763, Republic of Korea
*   Correspondence: hyounwoo@hanyang.ac.kr (H.W.K.); sangsub@inha.ac.kr (S.S.K.)

Abstract: Today, resistance gas sensors which are mainly realized from metal oxides are among the most used sensing devices. However, generally, their sensing temperature is high and other materials with a lower operating temperature can be an alternative to them. Graphene and its derivatives with a 2D structure are among the most encouraging materials for gas-sensing purposes, because a 2D lattice with high surface area can maximize the interaction between the surface and gas, and a small variation in the carrier concentration of graphene can cause a notable modulation of electrical conductivity in graphene. However, they show weak sensing performance in pristine form. Hence, doping, and in particular N doping, can be one of the most promising strategies to enhance the gas-sensing features of graphene-based sensors. Herein, we discuss the gas-sensing properties of N-doped graphene and its derivatives. N doping can induce a band gap inside of graphene, generate defects, and enhance the conductivity of graphene, all factors which are beneficial for sensing studies. Additionally, not only is experimental research reviewed in this review paper, but theoretical works about N-doped graphene are also discussed.

Keywords: graphene; reduced graphene oxide; nitrogen; doping; DFT; gas sensor

1. Introduction

Gases are found everywhere and we cannot imagine life without them. However, some gases and organic volatile compounds (VOCs) such as NO_2, CO, C_6H_6, and C_7H_8 are highly hazardous and their emission into the air leads to air pollution and subsequent problems related to human health. Today, due to the presence of many industries and plants and a large amount of car traffic, access to clean air is difficult; more than 90% of people live in cities with air pollution and, inevitably, they suffer from polluted air. Indeed, air pollution is one of the causes of premature death and sickness globally, and in total, it causes 16% of deaths in the world [1]. While the presence of some gases contributes to air pollution and health problems, some other gases such as H_2S are considered biomarkers for the diagnosis of some diseases such as halitosis and Down syndrome [2].

Humans have a sophisticated olfactory system which is constructed from millions of receptor cells (Figure 1). When odorant molecules come into contact with olfactory receptors through the glomerulus, mitral cells send a signal to the brain which will be detected. Hence, we are able to sense hundreds of smells easily and instantly. We can even instantaneously sense very low concentrations of odorants. For instance, we can detect methanethiol in 1 in 2.5 billion units of air [3].
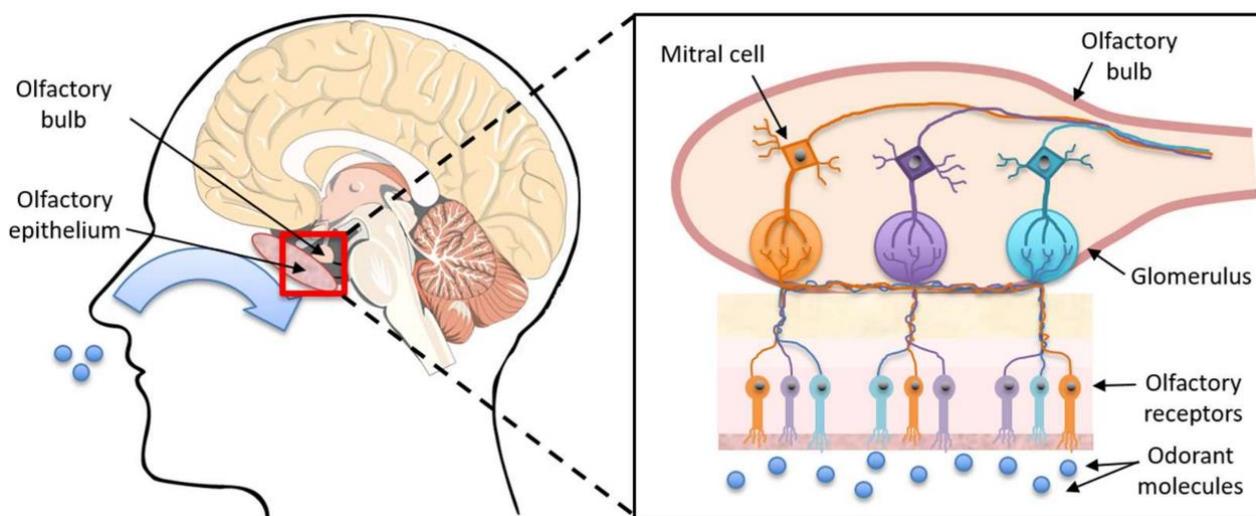
Figure 1. Olfactory system. Reprinted with permission from Ref [4]. Copyright 2018, MDPI.

However, in the case of odorless gases and substances such as CO, or extremely low concentrations of gases, we are unable to detect them. Moreover, people cannot be present everywhere. Standardized techniques for the detection of gases such as high-performance gas chromatography and ion chromatography need complex preparation, expensive and large equipment, and cannot provide fast results [5]. Hence, the realization of fast dynamics and stable gas sensors to detect low amounts of gases is of importance [6]. Considering these factors, various gas and humidity [7,8] sensors have been introduced which are fabricated from different materials with different sensing principles.

In general, gas sensors are electronic devices which can sense the presence of a target gas in their surrounding atmosphere and generate an electronic signal based on the nature and concentration of the target gas. Resistance or resistive sensors are, nowadays, highly well-liked thanks to their low cost, simple operation, ease of fabrication and measurement, high response, high stability, ease of integration, etc. [9]. In [10], Bradeen and Bradeen were the first to discover the effect of the surrounding atmosphere on the electrical properties of germanium [11]. Later, gas explosions in Japan inspired scientists to develop high-sensitivity gas sensors, and Seiyama et al. [12] introduced the first resistance gas sensor using ZnO for the detection of C_7H_8, CO_2, and propane gases. Additionally, Taguchi significantly worked on the development of resistive gas sensors and, finally, he commercialized the first resistive gas sensor based on SnO_2.

Mostly, resistive gas sensors are fabricated from semiconducting metal oxides. Nonetheless, they generally show unacceptable selectivity and should be heated to high temperatures to offer their best performance, especially when they are in pure form [13]. Thus, other materials such as conducting polymers (CPs) [14], carbon-based materials [15], MXenes [16], and metal chalcogenides [17] have also been employed for the realization of gas-sensing devices. Most of these materials can work at low or room temperature, which is a great advantage as it can remarkably decrease the power consumption of fabricated gas sensors. Generally, there are two common configurations for resistive gas sensors: planar and tubular. In both configurations, the sensing layer is deposited on the sensor substrate which is an insulating material, such as alumina equipped with conductive electrodes such as Au and Pt. Additionally, to provide temperature to the gas sensor, a heater is attached on back of the sensor for planar gas sensors (Figure 2), while for tubular gas sensors, generally, heater wire is put inside of the tube and by applying voltage to it, heat is generated via the Joule heating effect.
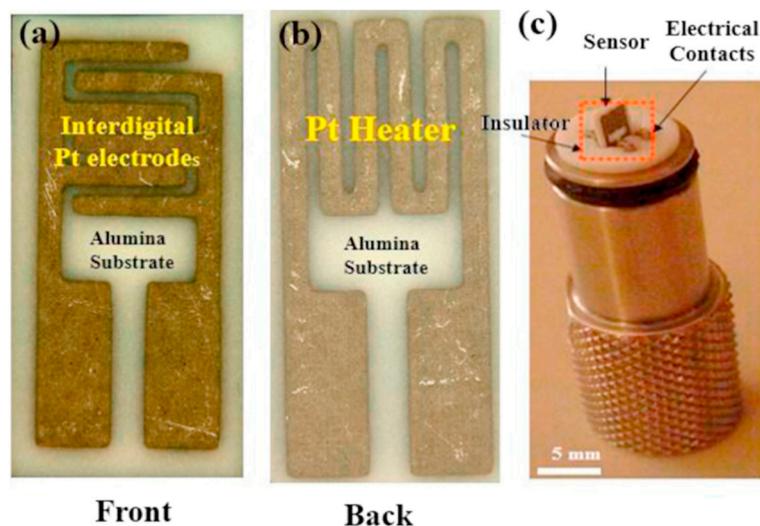
Figure 2. (**a**) Front side and (**b**) back side of alumina substrate equipped with electrodes and heater. (**c**) sensor holder. Reprinted with permission from Ref. [18]. Copyright 2016. Elsevier.

Thanks to the outstanding progress in the synthesis and discovery of new materials, nowadays, there are many engineering materials with unique features. Among them, carbon-based materials have high potential for sensing studies thanks to their good conductivity, high mechanical properties, relatively low prices, numerous varieties, and high chemical stability [19]. Among the different carbon allotropes, graphene with a 2-dimensional (2D) morphology, which was isolated from graphite in 2004 [20], is one of the most fascinating materials. Graphene refers to a single layer of "C" atoms which are arranged into a 2D honeycomb structure, and it is regarded as a basic building block for graphite (3D), carbon nanotubes (1D), and fullerenes (0D) [21] (Figure 3).
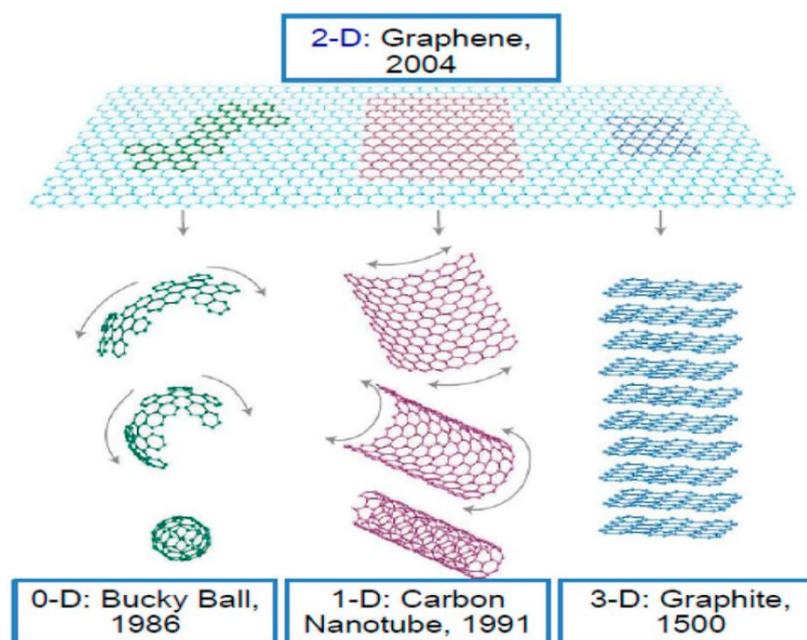

Figure 3. Different structures of graphene. Reprinted with permission from Ref. [22]. Copyright 2022. MDPI.

Nowadays, graphene can be easily synthesized; however, it is easily agglomerated due to Van der Waals interactions. Unfortunately, graphene suffers from the lack of band gap, which limits its application as a gas sensor, especially in pristine form. Furthermore,

it has poor water solubility. Hence, it can be partially oxidized by powerful oxidants and, in this way, graphene oxide (GO) is synthesized and different functional groups such as epoxy groups on its surface lead to water solubility. Due to the presence of carboxyl, carbonyl, and epoxide groups on the surface of GO, it is an electrical insulator because of the disruption of its sp^2 bonding networks [23,24]. Therefore, it has limited potential for gas-sensing purposes.

Reduced graphene oxide (rGO), a reduced from of graphene oxide (GO), can also be considered as promising material for gas-sensing applications, mainly thanks to having many functional groups and defects on it [25]. However, even though an exact comparison between N-doped graphene and rGO is difficult, rGO has no band gap, whereas N-doped graphene has a small band gap. Additionally, N-doped graphene has greater electron mobility than rGO. Furthermore, N-doped graphene may provide more active sites for gas molecules than rGO. In both materials, however, there are more defects than pristine graphene [26,27].

Referring back to graphene, it has been considered for different applications (Figure 4) thanks to its nontoxicity, high transparency, high mechanical properties, high electrical and thermal conductance, and high carrier mobility at room temperature [28]. Accordingly, it has been used in different areas such as gas sensors [29].
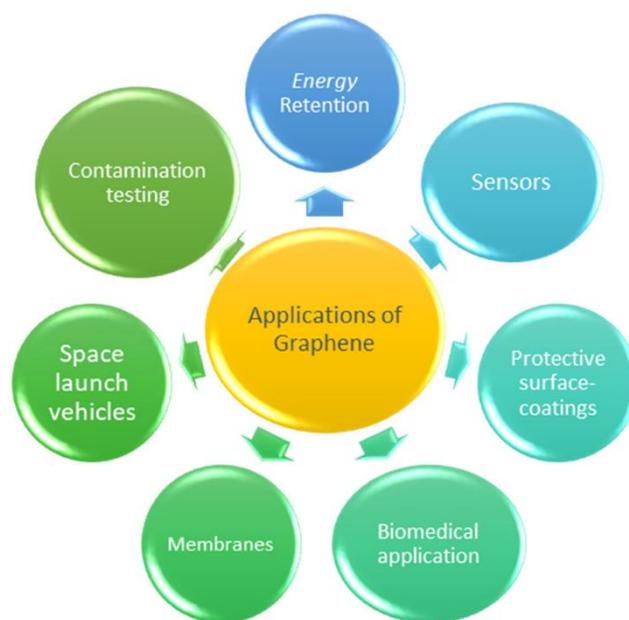

Figure 4. Different applications of graphene. Reprinted with permission from Ref. [30] Copyright 2021, Elsevier.

Generally, doping is a good technique to modify the features of different materials [31]. There are two types of doping in graphene. Metallic-cluster-induced doping, gate-controlled doping, or substrate-induced doping are known as electrical doping. Indeed, this type of doping does not affect the composition of graphene. Another type of doping, namely chemical doping, tunes the lattice structure via chemical routes such as substitution with foreign atoms [32].

Chemical doping can be distinguished as: (i) surface transfer doping, which happens when functionalized groups on the graphene surface are added; (ii) substitutional doping where the "C' atoms in graphene are replaced with another atom. N-type and p-type conductivity in graphene can be realized by substitutions of the atoms with more and fewer valence electrons than "C" atom, respectively. The presence of dopant leads to the opening of a band gap, converting graphene into a semiconductor. Moreover, depending on the type and amount of dopant, the position of Fermi level shifts, leads to a modulation of

electrical conductivity [33]. Opening the band gap and changing the conductivity through dopants are feasible strategies to control the electrical characteristics of graphene [34].

In particular, substitutional doping leads to the disruption of the sp^2 hybridization of the "C" atoms, resulting in a remarkable modulation of electrical properties [32]. For pristine graphene, since bonding (π) and antibonding (π*) orbitals touch at Brillouin zone corners, no band gap is observed in it (Figure 5). In fact, delocalized π electrons contribute to the conductivity of graphene; therefore, the dopant and defect sites will change its electrical features. Through the addition of dopant atoms, its original lattice symmetry will be broken, leading to the formation of a gap (Figure 5). The band gap is proportional to the dopant concentration, and in this way, the band gap can be tuned. Pristine graphene is chemically inert because its unpaired electrons are firmly bound and passivated in its delocalized π system. Although, some weak interactions and adsorption via a π-π, π–CH, or π-cation interactions are possible. The introduction of a dopant atom can lead to the generation of highly abundant active sites in graphene. Indeed, a dopant atom with a different electronegativity than "C" breaks the electroneutrality in graphene and forms unbalanced locally charged areas, where they play the role of active sites in graphene. Additionally, unpaired electrons in dopants lead to a localized distribution of molecular orbitals, inducing more chemical reactivity in graphene. Furthermore, active sites can be viewed as structural defects, which are formed due to the size difference and resultant lattice strain in graphene [33]. Therefore, doping in graphene can alter its electrical properties, induce structural defects, and increase its reactivity. This has led to the application of doped graphene in the gas-sensing area [35,36].
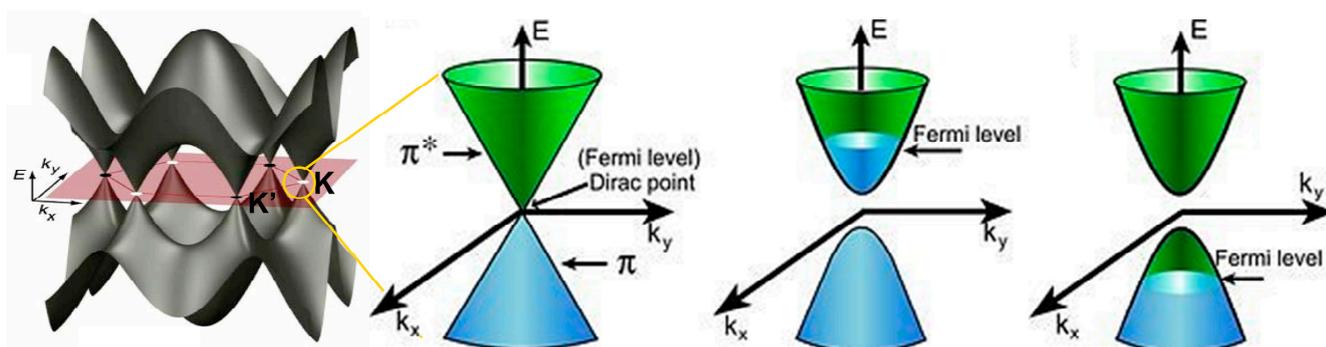

Figure 5. Left: The π* and π band dispersion of pristine graphene in the Brillouin zone. Right: the linear energy bands at the Dirac point and the Fermi level position as a function of doping. Reprinted with permission from Ref. [33]. Copyright 2015, Elsevier.

The B and N atoms have similar sizes to the "C" atom and are the main dopants in graphene. Their incorporation in graphene leads to hole acceptor and electron donor characteristics, respectively [37]. In particular, the "N" atom has an atomic radius of 0.70 Å, which is close to that of the "C" atom (0.77 Å). Furthermore, "N" has a higher electronegativity (3.04) than "C" (2.55). Moreover, "N" can form strong bonds with "C" atoms [38,39]. In this way, a more stable structure can form [40]. N doping in graphene not only enhances charge carrier mobility, but also makes it more hydrophilic as well as generating more active sites [38]. Additionally, N doping can remarkably improve the conductivity [41] and can enhance the biocompatibility of graphene [42]. Accordingly, N-doped graphene or its derivatives are used in electromagnetic wave absorption [43], electrochemical sensors [44], biosensors [45,46], gas sensors [47], electrocatalysts [48,49], solar cells [50], supercapacitors [51], energy conversion [52], and energy storage [53].

Until now, many attempts have been conducted for the controllable synthesis of N-doped graphene. In general, three N species as dopants can be discriminated in graphene. Figure 6: (i) graphitic N in which N atoms are substituted in the hexagonal shape on the internal parts of graphene, and (ii) pyridinic (iii) and pyrrolic, in which both types exist at edge defects [54].
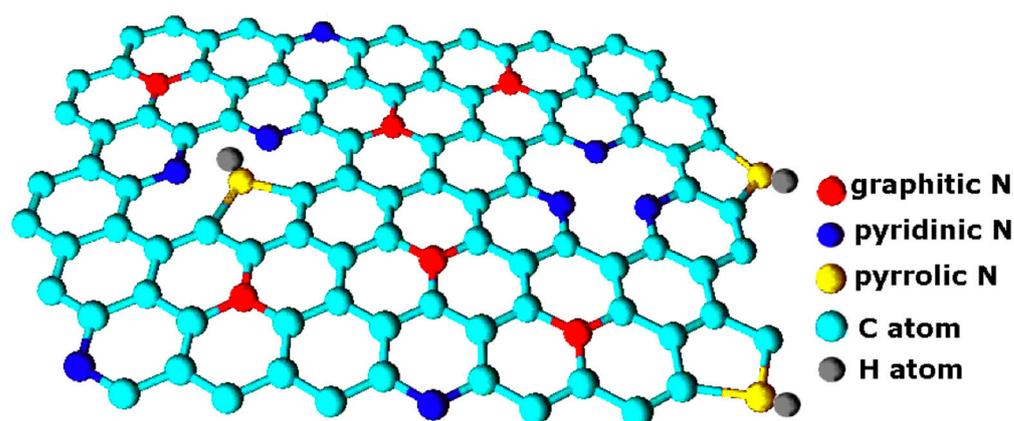
Figure 6. Three configurations of N atom in graphene. Reprinted with permission from Ref. [55]. Copyright 2020, MDPI.

To achieve the improved electrical properties, the "N" atom should be in the graphitic state. Anyway, other configurations of "N" as a dopant are also almost always present. Therefore, their presence and concentrations can also affect the physicochemical properties of doped graphene. Thereby, during the synthesis of N-doped graphene, the goal is having more graphitic "N" and less pyridinic and pyrrolic "N". When "N" is in the graphitic position, n-type doping is observed, while pyridinic and pyrrolic configurations will result in the p-type doping of graphene [55].

In the graphitic configuration, graphitic N is bonded to three other adjacent C atoms in the hexagonal ring and the excess valence electrons of N is delocalized, thus leading to an n-type doping effect. In the pyridinic N, two electrons fill σ-bonds with "C" neighbors, two electrons form a lone pair in the graphene plane, and the remaining electron occupies the N π-state. Hence, it has the equivalent occupation of a nominal "C" in graphene, but a π-electron is missing because of the vacancy site so the system is p-doped. In a similar way, pyrrolic N forms one σ-bond with its "C" neighbor and also forms σ-bonds to two H atoms. Two electrons go into the π-network, but similar to the pyridinic N case, the missing π-electrons from the divacancy sites accommodate this type of dopant, resulting in overall p-type doping [56,57].

There are various synthesis methods for the preparation of graphene (Figure 7) and most of them can be applied to synthesising N-doped graphene and its derivatives.
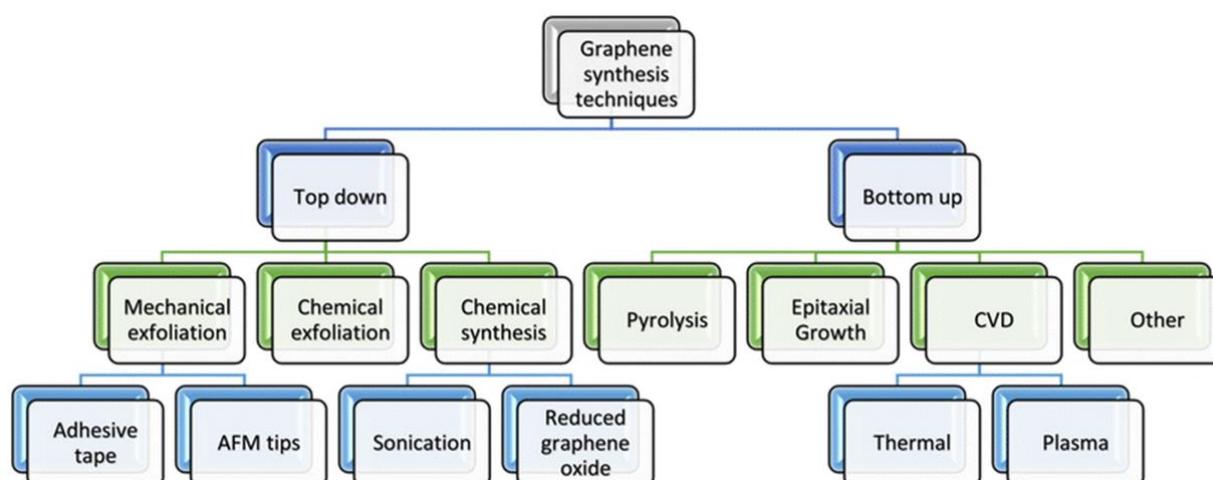

Figure 7. Some of the most common approaches for synthesis of graphene. Reprinted with permission from Ref. [58]. Copyright 2016, Springer.

Arc discharge [59], chemical vapor deposition (CVD) [60], the hydrothermal route [61], sonochemistry [62], ball milling [63], plasma treatment [64], thermal annealing [65], pyrolysis [66], and the hydrazine hydrate (N_2H_4) method [67] are among the most widely used approaches. These methods produce N-doped graphene with different configurations and different numbers of graphene sheets. The costs of the precursors, the thickness of the graphene sheets, the amounts and types of defects, ease of fabrication in terms of synthesis temperature and time, reproducibility, and production scale [68] are the main factors for the selection of a synthesis method. For example, CVD is one of the most promising methods for the fabrication of high-quality and large-scale graphene. Nonetheless, the required temperature for growth is high (~1000 °C) [69]. Details of the synthesis methods are beyond this review paper and interested readers can refer to a recent review by Yadav et al. [70] about the synthesis methods of N-doped graphene. Additionally, the characterization techniques for graphene and N-doped graphene are presented in detail in [40,71,72].

2. N-Doped Graphene and Its Derivatives as Resistive Gas Sensors: Theoretical Studies

With the progressive advancement of computational power and the availability of better supercomputers, theoretical studies of materials have become more feasible. Since gas sensor reactions include chemical reactions in which bonds are formed or broken and often result in a transfer of charge, the first principle (ab initio) or a quantum approach is preferred over a classical mechanics method. Quantum approach methods are useful for studying gas–surface interactions owing to their ability to model the adsorption mechanisms, the adsorption energy, charge transfer, electronic modification after gas adsorption, the structural changes, and the electronic properties involved. In this regard, density functional theory (DFT) calculations are considered a powerful technique to carry out many simulations, including the gas-sensing capability of different materials, without any side effects. DFT calculations are required for understanding experimental results at the molecular level, or as a predictive tool for the design of new sensing materials [73–75].

The adsorption of some gases, namely CO, NO, O_2, and NO_2, on defective graphene and N-doped graphene was investigated through DFT calculations. It was theoretically revealed that all CO, NO, and O_2 gases were chemisorbed on the defective graphene with large charge transfers. This can lead to the poor selectivity of CO in the presence of other gases. In contrast, only CO molecule with a large charge transfer was chemisorbed on the N-doped graphene, while other gases were only weakly adsorbed on it, reflecting good selectivity for CO gas sensing. Hence, through DFT calculations, it was shown that with a simple doping of "N" in a graphene lattice, it is possible to improve the selectivity to CO gas [76].

Based on DFT studies, the adsorption of CO molecules on pristine, N-doped, as well as Al-doped graphene was studied. The results showed that the most stable adsorption configuration was on top of a carbon (N or Al) atom of graphene sheets. The adsorption energies of CO molecules on pristine, N-doped, and Al-doped graphene were -0.01 eV, -0.03 eV, and -2.69 eV, respectively. In fact, the adsorption of CO molecules on pristine and N-doped graphene was physical adsorption, while it was chemisorbed on the Al-doped graphene. Moreover, calculations on band structure, density of states (DOS), and differential charge density showed that the adsorption of CO on Al-doped graphene was remarkably different from other materials in their study [77]. In another work, the adsorption of HCHO on Si-, Al-, Cr-, B-, N-, Au-, and Mn-doped graphene was studied using DFT calculations. It was reported that the HCHO molecule was weakly adsorbed on B- and N-doped graphene, while HCHO chemisorption was predicted on Si-, Al-, Cr-, Mn-, and Au-doped graphene. Additionally, based on adsorption geometries, charge transfers, adsorption energies, and density of states, it was found that Al and Mn dopants are the best ones for sensing enhancement towards HCHO gas [78]. The next work was related to an adsorption study of CO_2 on the P-, N-, B-, and Al- doped monovacancy graphene through DFT calculations. The band gap was changed from 0.004 to 0.478 eV and the electrical conductivity was changed from metallic to semiconducting when a monovacancy was

created in graphene. Furthermore, the doped graphene had a larger band gap relative to its undoped counterpart. The authors reported that Al-doped monovacancy graphene was better than other gas sensors for CO_2 gas sensing due to the suitable adsorption strength and band gap. Before the adsorption of CO_2 gas, the band gaps of N-doped monovacancy graphene and P-doped monovacancy graphene had no change, but those of B-doped monovacancy graphene and Al-doped monovacancy graphene changed. The band gap of Al-doped monovacancy graphene changed from almost 0 to 0.229 eV [79]. Hence, the electrical features were significantly changed, showing the high potential of Al-doped monovacancy graphene for CO_2 gas-sensing application.

BF_3 and BCl_3 are colorless gases and useful reagents in organic synthesis [80]. The energetic and electronic properties of pristine and N-doped graphene upon the adsorption of BCl_3, $B(OCH_3)_3$, and BF_3 gases were studied using DFT calculations. The computed dipole moment revealed that the amount of change in dielectric of the sensing material depends on the type of molecule. Furthermore, it was reported that N-doped graphene had much higher adsorption energy and higher net charge transfer relative to pristine graphene thanks to Lewis acid–base interactions between these gases and the sensing material. Additionally, the Lewis acidity increased as follows: $BF_3 < BCl_3 < B(OCH_3)_3$ with adsorption energies of -8.7, -18.3, and -26.5 kJ/mol, respectively, revealing better adsorption of the $B(OCH_3)_3$ on the N-doped graphene. Furthermore, very low adsorption energies were calculated on pristine graphene, suggesting a poor sensing response of pristine graphene to these gases [81].

The interactions of graphene and H_2 gas molecules can be controlled by adding dopant atoms. In this regard, Zhang et al. [82] explored the effect of Ti, Zn, Zr, Al, and N dopant atoms on the H_2 molecule adsorption of graphene through DFT calculations. It was indicated that the Ti-doped graphene had the highest interaction energy with the H_2 molecules (-0.299 eV), while those for Zn-doped and Al-doped graphene were -0.294 eV and -0.13 eV, respectively. However, the adsorption energy of H_2 molecules on N-doped graphene was much lower, namely -0.074 eV. Therefore, the N dopant did not enhance the hydrogen molecule response. Additionally, the comparison of the isosurface of the total electron density of the samples (Figure 8a–f) indicated that the interaction of the H_2 molecule with Ti-doped graphene had the largest isosurface area. Interestingly, the doped N atom did not affect the electronic features of graphene. Indeed, no electron accumulation was seen on the N-doped graphene, while the Ti-doped one exhibited the highest electron loss upon interaction with H_2 gas (Figure 9a–f).

In an interesting work, Zhang et al. [83] reported the effects of doped Ti or N atoms on the interaction of CO, NO, SO_2, and HCHO gases with graphene through DFT calculations. The adsorption energy, electron density difference, and density of state studies exhibited that the Ti dopant could improve the interaction of gases with graphene. By contrast, the interaction energy between the gas molecules and the N-doped graphene was weaker relative to the Ti-doped graphene. Additionally, the Ti-doped one showed a stronger interaction with SO_2 gas and the weakest interaction with CO gas, suggesting good potential for Ti dopant in graphene for SO_2-sensing studies. Wang et al. [84] studied the adsorption of NO_2, NO, and NH_3 molecules on B-doped and N-doped graphene through a DFT study. They built their models by putting these gases on three different high-symmetry adsorption sites. It was indicated that NO/NO_2 gases had more stability on B-doped graphene than those on N-doped graphene. Additionally, the detection of a NH_3 molecule on B- or N-doped graphene was rather weak, suggesting that this gas cannot effectively adsorb on the surface of these sensing materials. As a pollutant, chloroform ($CHCl_3$) has strong volatility and is carcinogenic. Furthermore, it can lead to water pollution [85]. Tian et al. investigated the adsorption of chloroform on N-doped and Al-doped graphene using DFT studies [86]. The configurations of pristine and N-doped graphene did not change, while the adsorption of $CHCl_3$ caused a structure change in Al-doped graphene. It was revealed that there is more charge transfer, a smaller adsorption distance, and larger adsorption energy upon the

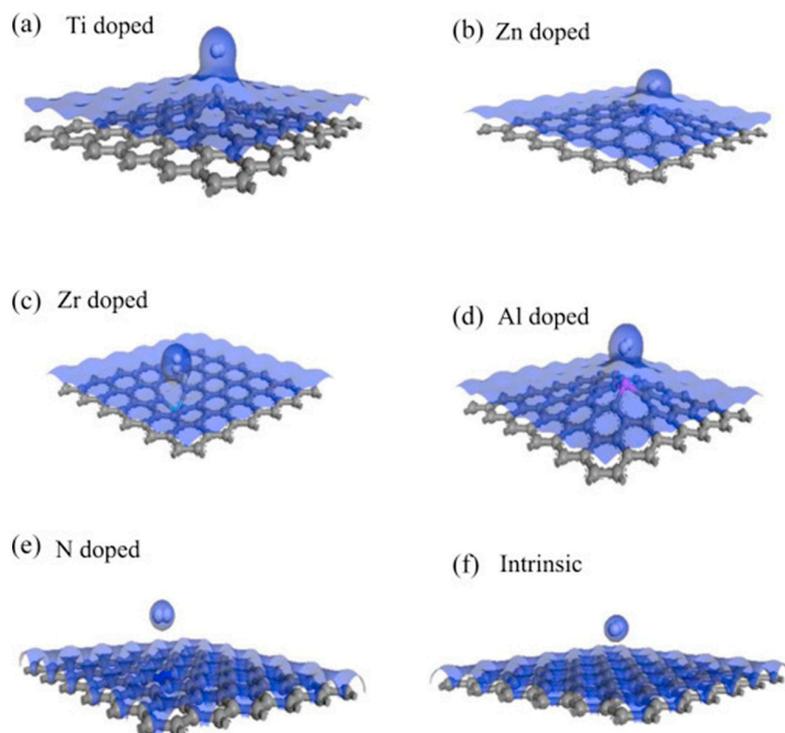adsorption of CHCl$_3$ on Al-doped graphene relative to adsorptions on pristine graphene and N-doped graphene.

Figure 8. Isosurface of electron density of H$_2$ adsorption on doped (**a**–**e**) and (**f**) pristine graphene. Reprinted with permission from Ref. [82]. Copyright 2013, Elsevier.
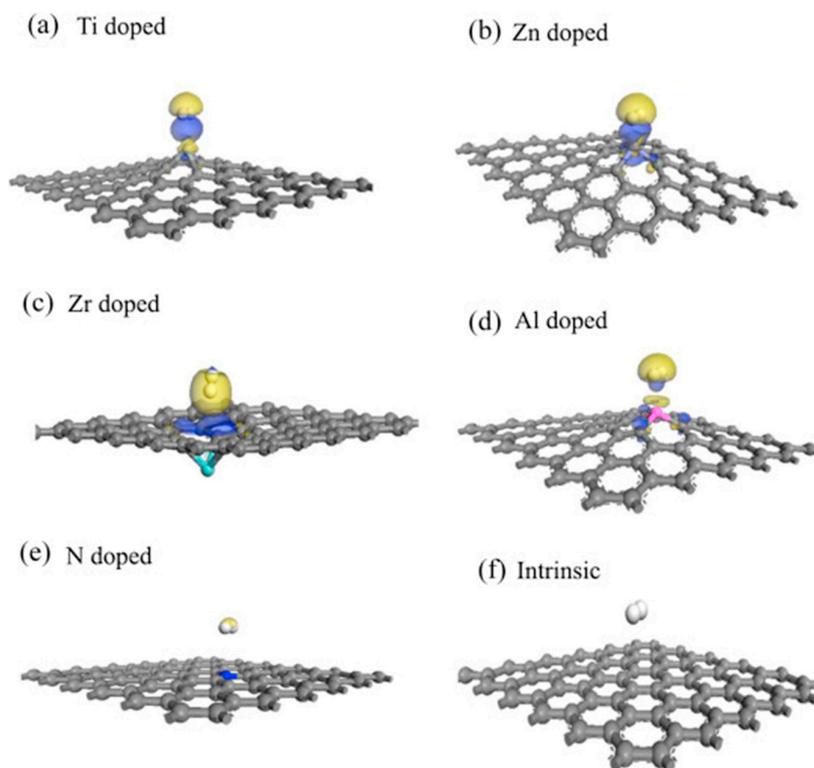

Figure 9. Electron density difference of H$_2$ adsorption on doped (**a**–**e**) and (**f**) pristine graphene. Reprinted with permission from Ref. [82]. Copyright 2013, Elsevier.

Shokuhi Rad et al. [87] investigated the adsorption of SO_2 and SO_3 gases on graphene and N-doped graphene by means of DFT calculations. SO_2 and SO_3 molecules were physically and chemically adsorbed on the surface of N-doped graphene, respectively, whereas almost no adsorption was generated on the pristine graphene. This suggests the possibility of using N-doped graphene for SO_3 sensing in real applications. Zhang et al. [88] investigated the adsorption of NO_2, NO, and O_2 gases on Ti- or N-doped graphene using the DFT method. The results revealed that the interactions between the above gases and Ti- or N-doped graphene were unaffected by the size of the graphene. The Ti doping improved the interactions between the gases, while the N doping had no significant effect on the interactions. In particular, the Ti doping of graphene significantly enhanced the adsorption of NO_2 gas relative to pristine graphene. Additionally, the role of noble metal decoration on the adsorption of gases on graphene was investigated. Pd is a noble metal with good catalytic activity and a lower price than Pt [89]. Tang et al. [90] investigated the formation geometries and gas adsorption of a single Pd atom supported on divacancy graphene (555-777-graphene-Pd) and N_x-doped graphene (N_x-graphene-Pd, x = 1, 2, 3) through DFT calculations. The N_x graphene-Pd configurations had the smallest formation energies and among them, the N_3-graphene-Pd was easily formed. Additionally, the N_3-graphene-Pd exhibited better adsorption properties for NO_2 gas relative to 555-777-graphene-Pd. Additionally, the adsorption energy of NO_2 gas was larger than CO and O_2 gases.

Using vibrational spectroscopy, Carraro et al. [91] demonstrated that, upon "N" doping in graphene on Ni (111), two CO adsorptions are possible. The dominant one had a CO stretch frequency (256 meV) close to that (260 meV) for the pristine graphene/Ni (111) sample, while it had the same desorption energy. In contrast, the second species had a CO stretch frequency of 238 meV and ~50% larger desorption energy. It was related to CO-adsorbed molecules close to the N-doped sites of pyridinic and/or pyrrolic nature. Their work demonstrated the potential of N doping for the adsorption of CO with graphene on Ni (111).

Based on the DFT calculation results, it can be concluded that, overall, N doping can enhance the adsorption of gas molecules on graphene or rGO, relative to pristine (undoped) graphene or rGO. However, it should be also mentioned that, in comparison to metallic dopants such as Al, Ti, or even B dopant, generally, N-doped graphene shows weaker adsorption of the target gas molecules. However, the adsorption behavior of codoped graphene such as Ti/N, and codoping in graphene in general, need to be further explored using DFT calculations.

3. N-Doped Graphene and Its Derivatives as Resistive Gas Sensors: Experimental Studies

Graphene quantum dots (GQDs) have lateral dimensions smaller than 10 nm and the combination of QDs and graphene characteristics in these materials leads to revealing enhanced features such as low toxicity, chemical stability, high strength, tunable energy band gaps, outstanding optical properties, and excellent microelectronic properties [92]. In this regard, Masemola et al. [87] prepared a N-doped GQDs/PANI composite for ethanol-sensing studies (Figure 10).

The NGQDs/PANI sensor revealed a better response compared to that of pristine PANI (Figure 11) along with a faster response time and recovery time of 85 s and 62 s, respectively, to 100 ppm ethanol vapor at 25 °C. The enhanced response of the composite sensor was related to the incorporation of N in the GQDs. It was related to the enhanced conductive pathways between the PANI and N-doped GQDs, which induced conductive pathways created by strong synergetic effects through interchain π interactions between the NGQDs and PANI. Furthermore, the surface area of the composite sensor (41.0 m^2 g^{-1}) was higher than that of bare PANI (31.2 m^2 g^{-1}), leading to higher adsorption of ethanol molecules on the composite sensor.
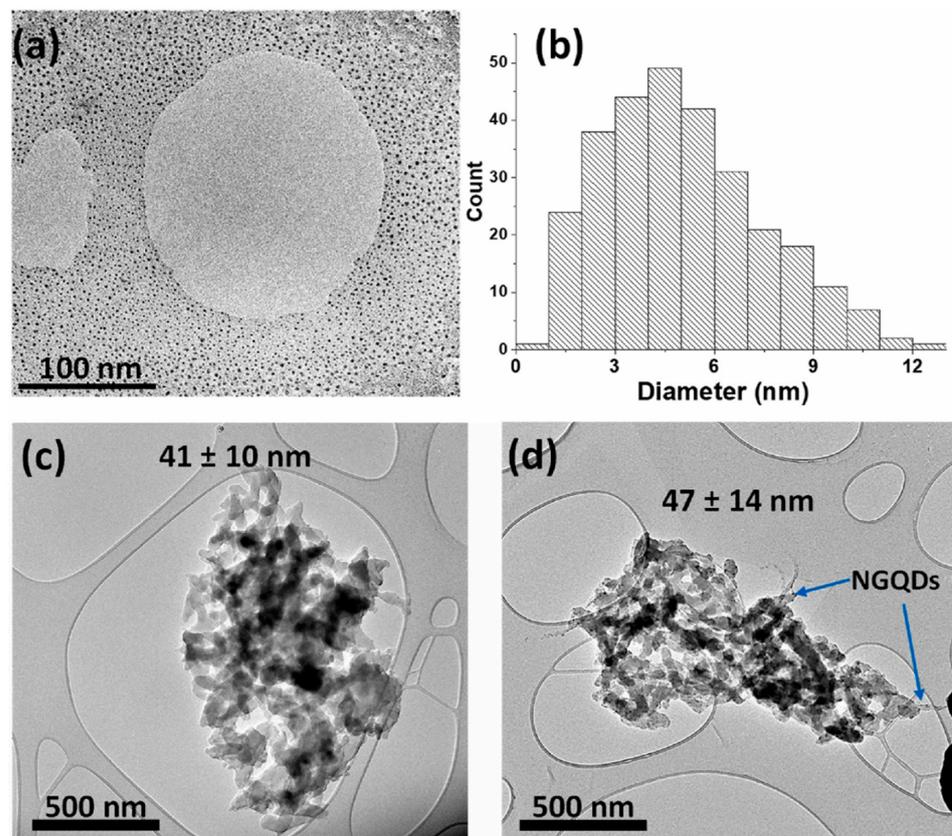
Figure 10. TEM images of (**a**) N-doped GQDs, (**b**) particle size distribution, TEM images of (**c**) PANI and (**d**) N-doped GQDs/PANI composite. Reprinted with permission from Ref. [93]. Copyright 2022, Elsevier.
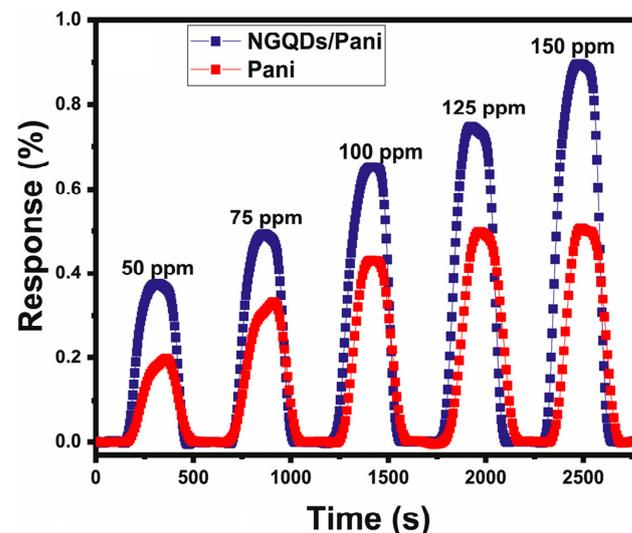

Figure 11. Dynamic resistance curves of PANI and N-doped GQDs/PANI sensors to ethanol at room temperature. Reprinted with permission from Ref. [93]. Copyright 2022, Elsevier.

CPs are used in gas sensors due their tunable properties, low cost, and room-temperature operation [94]. In another study, Gavgani et al. [95] realized VOC gas sensors based on pristine N-doped GQDs, poly (3,4 ethylenedioxythiophene)-poly(styrenesulfonate) (PEDOT-PSS), and N-doped GQDs/PEDOT-PSS nanocomposites. The fabricated sensors at room temperature were exposed to 100 ppm acetone, toluene, propanol, chlorobenzene,

methanol, ethanol, and water. It was reported that the N-doped GQDs/PEDOT-PSS nanocomposite gas sensor showed a good response to methanol, whereas it revealed almost no response to other gases. The response of the optimal sensor to 100 ppm methanol was 154.4%, which was 12 times as high as that of the PEDOT-PSS sensor. The sensing mechanism of the optimal sensor was described using the following reasons: (i) The swelling of CPs due to the diffusion of methanol into the CPs. In this case, the interchain distance of CPs increases and the electron hopping process becomes more difficult. (ii) N-doped GQDs integrated into the CP matrix acted as conductive paths, favoring the electron hopping. Therefore, a combination of the above two processes leads to the modulation of the electrical resistance in the presence of methanol gas.

Nitrogen dioxide (NO_2), with a highly toxic nature, emits from fossil fuels and can damage the human respiratory system [96]. In this regard, a series of N-doped GQD 3-dimensional ordered macroporous (3DOM) In_2O_3 composites were synthesized for NO_2 gas-sensing studies. The results showed that the sensor exhibited a better response to NO_2 gas with fast and recovery times and a low working temperature (100 °C), relative to pristine In_2O_3 and rGO/3DOM In_2O_3 sensors. Furthermore, it showed good selectivity and high long-term stability. The conductivity enhancement due to the presence of N-doped GQDs and the generation of heterojunctions between In_2O_3 and N-GQDs, as well as the presence of macrospores, accounted for the enhanced response to NO_2 gas [97].

P-type rGO and N-doped rGO were explored for NO gas detection at 25 °C. The response of the N-rGO sensor to 1000 ppb NO (1.7) was higher than that of the rGO sensor (0.012) and it was even able to detect 0.4 ppm NO gas. The increase in the NO gas-sensing performance was related to N doping. First, the N doping produced polarization in the sp^2 carbon network and further affected the physical and the electrical properties of the sensor. Second, the improved gas response was related to the improved active sites of pyridinic N and/or pyrrolic N. In particular, pyridinic N, where the N atom is bonded to two C atoms and donates one p-electron to the aromatic π system, modified the band structure of carbon and lowered the work function. Additionally, the electron density on the neighboring C atom decreased, which resulted in the transfer of electrons from the C to N atoms, and N back-donate electrons to the neighboring C pz orbitals. These processes facilitated the dissociation of oxygen molecules on the C atoms and helped to form a strong bond between O and C atoms [98].

TiO_2 is an n-type semiconductor which offers high chemical stability and excellent electronic properties. Yan et al. [99] investigated the sensing properties of C- and N-doped rGO/TiO_2 composites with special exposed facets synthesized via a hydrothermal method at 180 °C using HF. The gas-sensing performance of the N-doped rGO/TiO_2 sensor was better than that of the C-doped rGO/TiO_2. The N-doped rGO/TiO_2 sensor exhibited the highest response to isopropanol, ethanol, and acetone gases at 210, 240, and 270 °C, respectively. The N-doped rGO/TiO_2 sensor exhibited the highest response to 100 ppm acetone with a response of 14.12, while its responses to ethanol and isopropanol were 5.85 and 3.47, respectively. Figure 12a–d present the sensing performance of the sensors towards isopropanol. The N dopant led to a narrowing of the band gap of the composite and an improvement in the binding between N-doped rGO and TiO_2, which was useful for charge separation, more carrier concentration, and electron mobility. The TiO_2 in the composite generated electron–hole pairs, and the N-doped rGO inhibited the electron–hole pair recombination owing to the 2D planar π-conjugation. Hence, a prolonged lifetime of the charge carriers occurred and generated electron–hole pairs, which reduced oxygen to form radicals with a strong oxidation capability to react with gases. Additionally, rGO, with good electrical properties, led to the fast diffusion, capture, and release of electrons. Moreover, the presence of defects and functional groups in the N-doped rGO facilitated the gas adsorption.
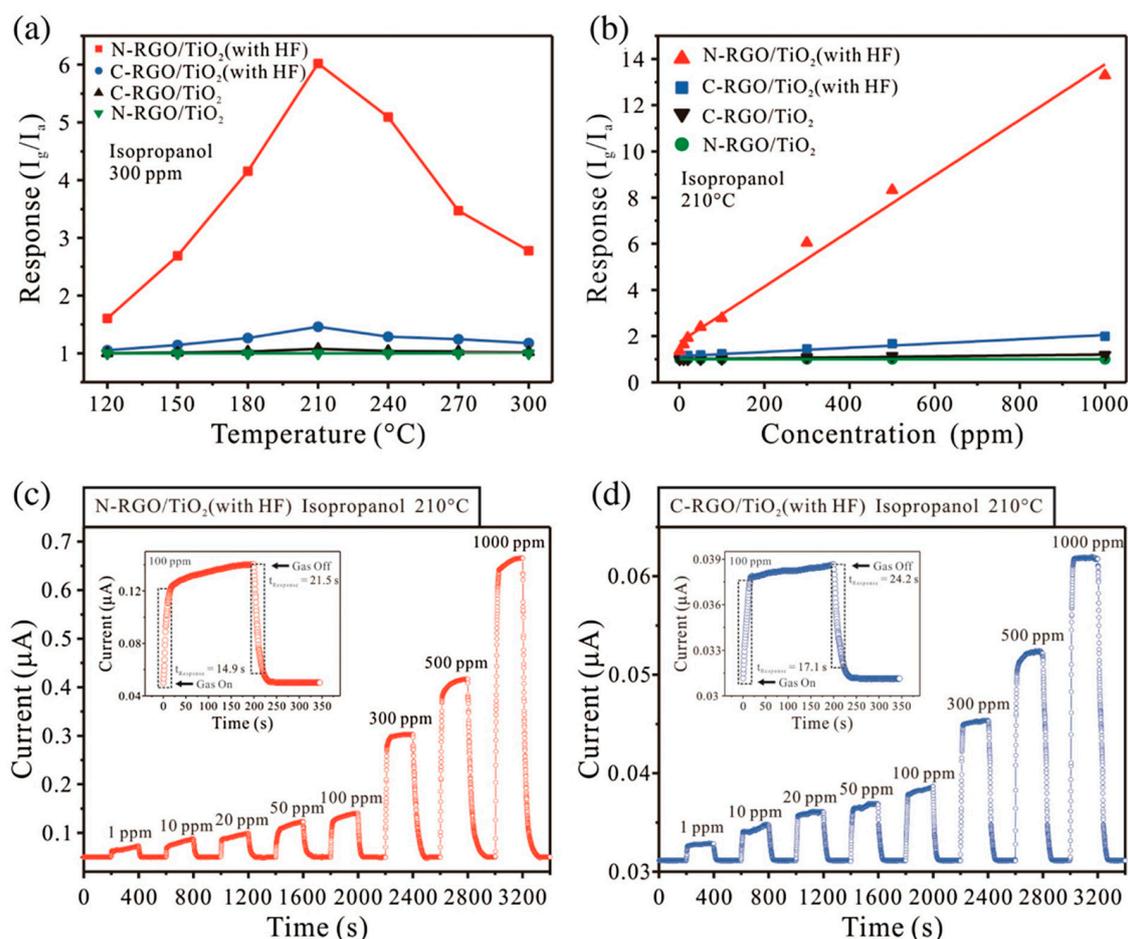
Figure 12. (**a**) Responses of different sensors to 300 ppm isopropanol versus temperature. (**b**) Calibration curves of different sensors to isopropanol at 210 °C. (**c**,**d**) Dynamic current curves of N-doped rGO/TiO$_2$ and C-doped rGO/TiO$_2$ sensors to isopropanol at 210 °C. Insets: Enlarged part of the (**a**) N-doped rGO/TiO$_2$ and (**b**) C-doped rGO/TiO$_2$ plots to 100 ppm isopropanol at 210 °C. Reprinted with permission from Ref. [99]. Copyright 2016, Elsevier.

Lin et al. [100] fabricated mesoporous p-type Co$_3$O$_4$/N-doped rGO nanocomposites via a metal–organic framework (MOF) template. Elemental mapping revealed the uniform distribution of Co, O, C, and N elements in the sample (Figure 13). The effect of initial rGO concentration on the gas-sensing characteristics of the composite sensor was studied. It was found the Co$_3$O$_4$/N-doped rGO-0.5 (rGO mass = 0.5 mg) nanocomposite sensor had a better response to ethanol than other sensors, and a response of 44.5 to 200 ppm ethanol at 200 °C was obtained (Figure 14). The enhanced sensing response was related to the presence of rGO with high electron mobility, which facilitated the migration of carriers in the sensing process, leading to improved sensing performance. Furthermore, the coupling effect between Co$_3$O$_4$ and N-doped rGO enhanced the oxygen reduction ability in the gas-sensing process and increased the transfer rate of charge carriers. In addition, the sensor had a high specific surface area, and so provided more effective active sites during ethanol adsorption than the other samples. The N atoms were mainly bonded with rGO as pyridine-N. They were bonded with the "C" atoms of the rGO sheets, which provided lone pair electrons to increase the electronic partial density of states near the Fermi level. The higher density of states facilitated the electron flow during the sensing reactions.
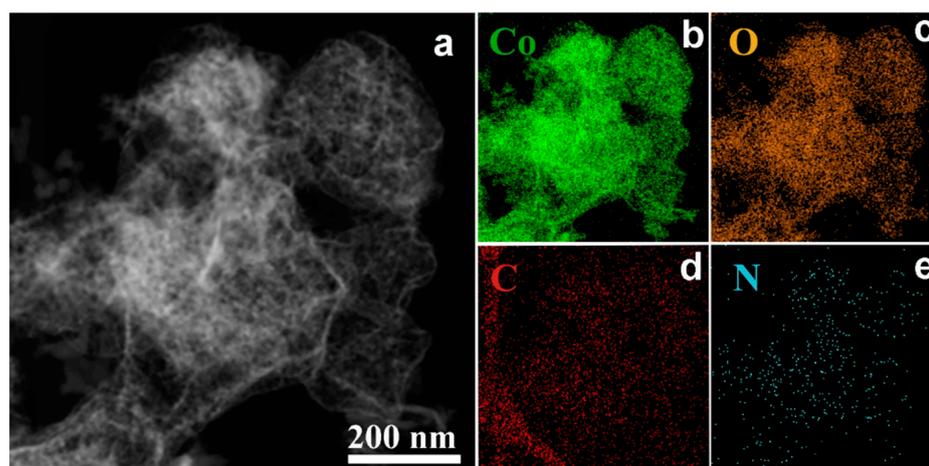
Figure 13. (**a**) STEM image and elemental mapping of Co_3O_4/N-doped rGO-0.5 (**b**) Co, (**c**) O, (**d**) C, (**e**) N. Reprinted with permission from Ref. [100]. Copyright 2020, Elsevier.
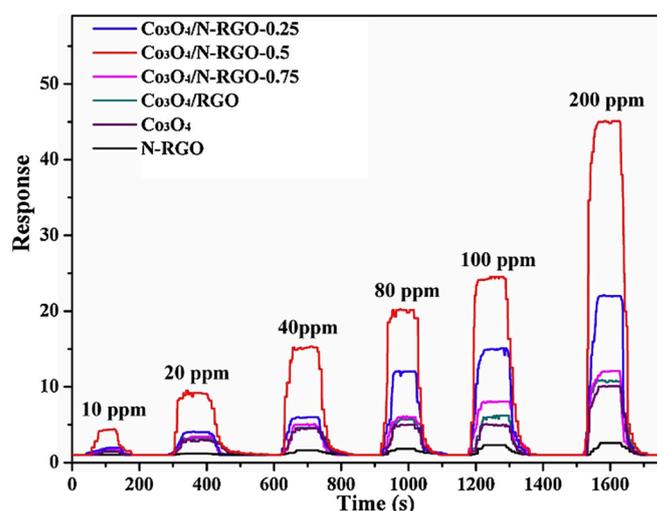

Figure 14. Response transients of different gas sensors to various concentrations of ethanol at 200 °C. Reprinted with permission from Ref. [100]. Copyright 2020, Elsevier.

Modak et al. [101] introduced NO_2 gas sensors using a SnO_2-N-doped rGO composite for NO_2 sensing. SnO_2-rGO composites with three amounts of SnO_2 (low, medium, and high) were synthesized via a hydrothermal reaction. The samples were coded as SR1, SR2, and SR3. For N-doped rGO, urea was used as a source of N atoms. They were coded as SRN1, SRN2, and SRN3 based on 0.09, 0.18, and 0.27 mg of urea, respectively. Figure 15 presents the responses of different sensors at different temperatures to 0.5 ppm NO_2 gas, where the SRN2 sensor revealed the highest response to NO_2 gas at 120 °C. Additionally, the doping of N atoms into rGO increased the sensor response to NO_2. However, high doping led to a decrease in the sensor response.

N doping led to the generation of more active sites which were beneficial for NO_2 adsorption. Additionally, the higher surface area and higher pore volume of the SRN2 sensor facilitated a higher response to NO_2 gas. Furthermore, the large number of defects and oxygen vacancies in SRN2 enhanced the gas response. Indeed, N-doped rGO had a greater number of defects in the rGO sheets, which acted as adsorption sites for the NO_2 gas. Additionally, the SRN2 sensor had higher conductivity compared to SR sensors, owing to the presence of a lone pair of electrons on the N atom.
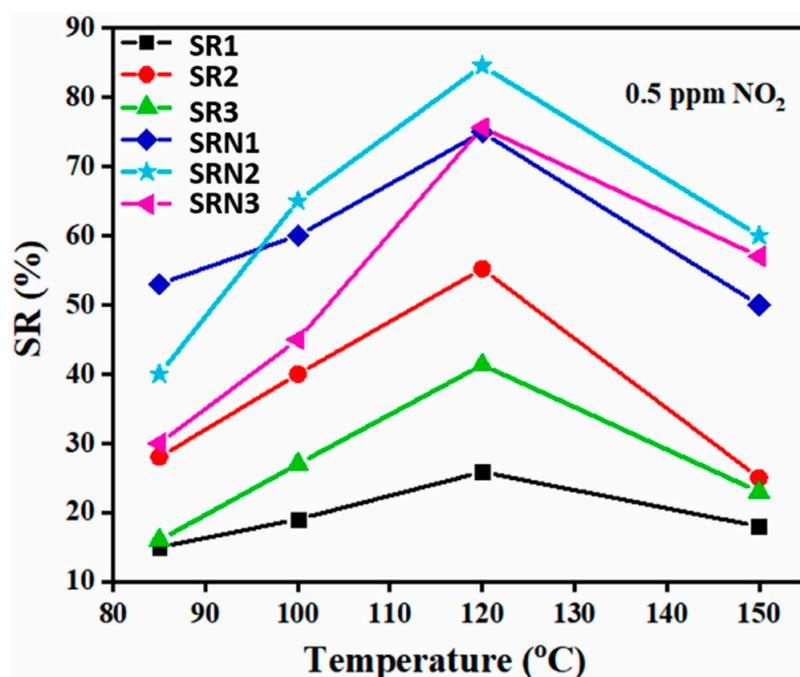
Figure 15. Response of different sensors to NO_2 gas versus temperature. Reprinted with permission from Ref. [101]. Copyright 2022, Elsevier.

As shown in Figure 16, due to the work function difference between SnO_2 (3.6 eV) and rGO (4.56 eV), the electrons moved from SnO_2 to N-doped rGO; thus, potential barriers were formed at the interfaces between SnO_2 and rGO in air (Figure 16a). rGO provided an electron conduction path owing to its high mobility of charge carriers. In NO_2 atmosphere, due to the abstraction of electrons by NO_2 gas, the height of the potential barrier increased (Figure 16b), contributing to the resistance change and appearance of a sensing signal.
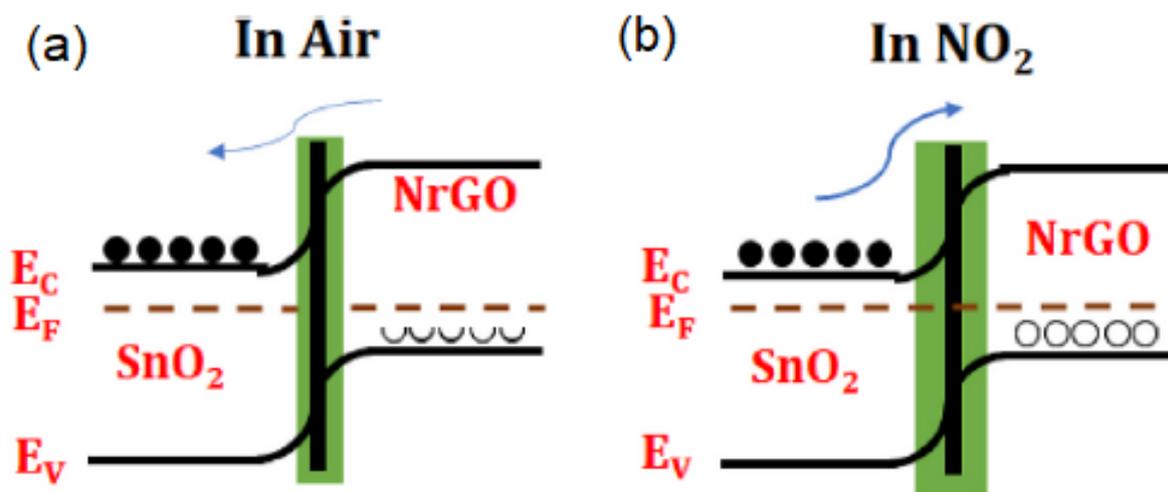

Figure 16. Sensing mechanism of SnO_2/N-doped rGO to NO_2 gas (**a**) after contact in air (**b**) after contact in NO_2 atmosphere. Reprinted with permission from Ref. [101]. Copyright 2022, Elsevier.

Nie et al. [102] synthesized N- and Si-codoped (N/Si-doped) graphene. The N atoms acted as the active sites for the NO_2 adsorption, whereas the Si atoms remarkably modified the electronic features of the graphene. The N/Si-doped graphene exhibited p-type conductivity, indicating that the hole doping from Si atoms overcame the electron doping from N atoms. The sensor was able to detect NO_2 gas at 25 °C.

NH$_3$, as a toxic gas, is an irritant to the eyes, skin, and respiratory system [103]. Among different CPs, PANI is popular thanks to merits such as the ease of synthesis, low cost, stability, and good response to NH$_3$. Nevertheless, in pristine form, it has a response [104]. Therefore, it is often used in composite form. In this regard, Gavgani and coworkers [105] introduced a flexible NH$_3$ sensor using a S/N-codoped GQDs/PANI composite. The response of the S/N-codoped GQDs/PANI sensor to 100 ppm NH$_3$ was 5-fold higher than that of the PANI sensor, with a faster response time and recovery time. Additionally, the S/N-doped GQDs/PANI hybrid gas sensor showed better selectivity to NH$_3$ gas relative to the PANI sensor (Figure 17).
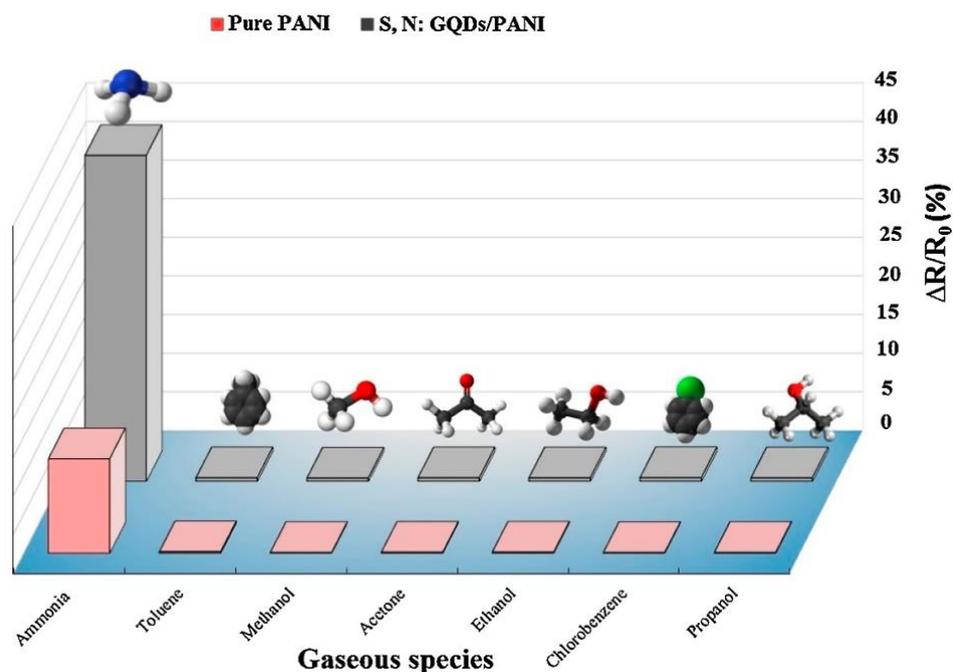

Figure 17. Selectivity patterns of pristine PANI and S/N-codoped GQDs/PANI sensors. Reprinted with permission from Ref. [105]. Copyright 2016, Elsevier.

The increased NH$_3$-sensing features were attributed to the swelling of the PANI in the presence of NH$_3$, as well as the reversible acid–base doping/dedoping of the PANI in the presence of NH$_3$ gas, which changed it from a conductive state to an insulating state, leading to an increase in the resistance and formation of heterojunctions between the PANI and the S/N-codoped GQDs.

In another study, an NH$_3$ gas sensor based on a combination of PANI and different amounts of N-doped GQDs was fabricated and Ag or Al was used for the electrodes. The sensor with Ag and Al contact showed Ohmic and Schottky behaviors, respectively. The sensor with a Ag electrode had a much higher response to NH$_3$ than that of the sensor with an Al electrode. The (50 wt%) N-GQDs/PANI sensor with a Ag electrode displayed a high response of 110.92 to 1500 ppm NH$_3$ at room temperature, which was around 30% higher than that of the Al electrode [106].

In another study, the sensing response of a PEDOT-PSS sensor to 1500 ppm NH$_3$ at room temperature increased from 30.13% to 212.32% with 50 wt% N-doped GQDs. Furthermore, the sensor with N-GQD showed faster dynamics and higher stability [107]. Purbia et al. reported N-doped GQDs/SnO$_2$ nanocomposites for the detection of NO$_2$ gas at 150 °C. The response to 100 ppb NO$_2$ gas was 292 with a response time of ~3 min. Furthermore, it revealed good selectivity to NO$_2$ gas. The formation of SnO$_2$-N-doped GQDs, the presence of defects, and the high surface area of the gas sensor led to a better response in the composite sensor relative to the bare SnO$_2$ gas sensor [108].

As far as we know, unfortunately, no paper discussing the effect of humidity on the gas-sensing properties of N-doped graphene has been published. However, for resistive gas sensors, it is generally accepted that the presence of water vapor decreases the sensing performance. In fact, since the sensor signal depends on the adsorption of the gases on the surface of the sensor, in a humid environment, some of the adsorption sites are occupied by water molecules, leading to a decrease in the sensing performance. However, specifically for N-doped graphene and its derivations, some studies on this aspect are necessary.

In Table 1, we summarize the gas-sensing properties of N-doped-graphene-based gas sensors. N-doped graphene or N-doped rGO, mostly in composites with metal oxides and CPs, have been used for sensing studies. Additionally, mostly NH_3 and NO_2 gases and VOCs such as ethanol, methanol, and isopropanol have been used as the target gases. With some exceptions, generally, the sensing temperature is low or at room temperature, and in comparison with other resistive-based gas sensors such as metal-oxide-based sensors, this is an advantage. However, the response time and recovery times are relatively long. In comparison with metal oxide gas sensors, the response values are generally lower. However, in some cases, very high responses have been reported.

Table 1. Gas-sensing performance of N-doped graphene and its derived gas sensors.

Sensing Material	Target Gas	Conc. (ppm)	Response *	T (°C)	Response Time (s)/Recovery Time (s)	Ref.
N-doped GQDs/PANI composite	Ethanol	100	0.7% $[(R_a - R_g)/R_a] \times 100$	25	85/62	[93]
N-GQDs/PEDOT–PSS nanocomposite	Methanol	50	140% $[\Delta R/R_a] \times 100$	25	12/32	[95]
N-doped GQD-(3DOM)–In_2O_3 composite	NO_2	1	82 R_g/R_a	100	~95/~36	[97]
N-doped rGO	NO_2	1000	1.7 R_g/R_a	25	~100/~20	[98]
N-doped rGO/TiO_2 nanocomposite	Isopropanol	300	6 I_g/I_a	210	~100/120	[99]
Co_3O_4/N-doped rGO nanocomposite	Ethanol	100	24.5 R_g/R_a	100	~20/~50	[100]
SnO_2-N-doped rGO	NO_2	0.5	85% $[\Delta R/R_a] \times 100$	120	22/125	[101]
S/N-codoped GQDs/PANI	NH_3	100	42.3% $[\Delta R/R_a] \times 100$	25	115/44	[105]
N-doped GQDs/PANI composite	NH_3	1500	110 R_g/R_a	25	~900/940	[106]
N-doped GQDs	NH_3	1500	212.32% $[\Delta R/R_a] \times 100$	25	900/910	[107]
N-doped GQDs/SnO_2 nanocomposites	NO_2	100 ppb	292 R_g/R_a	150	181/81	[108]

* Note: R_a: resistance in air; R_g: resistance in the presence of target gas. I_a: current in air; I_g: current in the presence of target gas.

Additionally, in Figure 18, we schematically represent the main features of N-doped graphene and N-doped rGO as gas sensors.
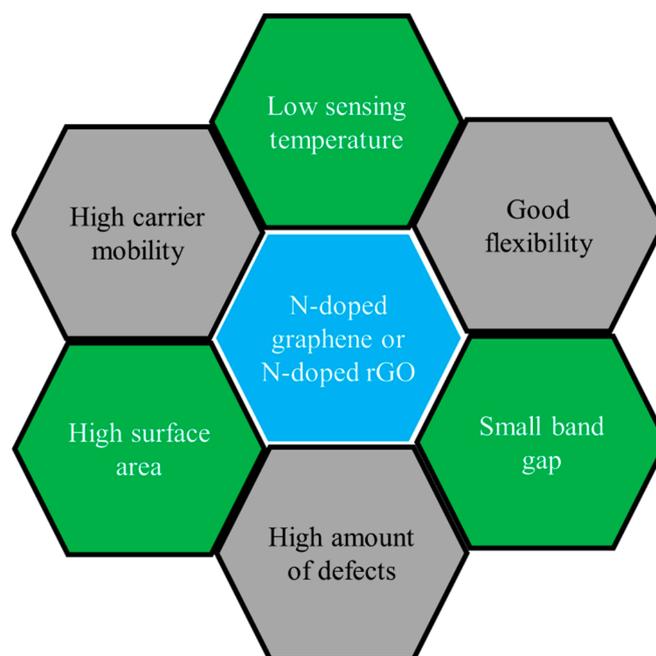
Figure 18. Main features of N-doped graphene and N-doped rGO as gas sensors.

4. Conclusions and Outlooks

We reviewed the gas-sensing characteristics of N-doped graphene and rGO resistance gas sensors. There are various methods to fabricate N-doped graphene or rGO. N doping in graphene and rGO can not only induce defects, but can also increase the electrical conductivity and induce n-type conductivity in graphene. Through N doping, it is feasible to tune the band gap of graphene and rGO. Furthermore, N dopants are cheaper than noble metals such as Au, Pt, and Pd.

Generally, N doping causes an enhanced gas response relative to pristine graphene and rGO. However, it seems that more studies are necessary in this context. Even though there are good examples from the literature of DFT calculation studies of N-doped graphene, they need parallel experiments to be verified. Additionally, as far as we know, no or only a few studies have been devoted to N doping in GO for sensing studies, and in this aspect, more experimental works are needed.

There are some experimental works that have studied N-doped graphene or rGO in composite form for gas-sensing studies. However, often, no optimization of the amount of N doping is reported and this aspect should also be considered. Additionally, there are only a few studies related to noble metal decoration on N-doped graphene or rGO. For example, Au or Pd loading on N-doped graphene or its derivatives is expected to improve the gas-sensing performance. It seems that the synergetic effect of N doping and noble metal decoration can significantly promote the sensing performance. In future studies, it seems that the following directions in this area are necessary:

(i) Optimization of the amount of N doping in graphene and rGO: Only a few papers mentioned the optimization of N doping in rGO. Generally, there is a volcano-shape dependency of the sensing response with respect to the amount of N doping. Therefore, at very low and very high amounts of doping, the sensing performance decreases. Hence, it is important to find the optimal value of N doping, where the maximum sensing response can be achieved.

(ii) The study of N-doping effect in GO for gas-sensing studies: As far as we know, there is no study about the effect of N doping on the gas response of GO gas sensors. Hence, we think that this aspect needs some studies. In fact, N doping will increase the conductivity of GO, and in this way, it is expected that the gas-sensing performance will be increased after N doping in GO.

(iii) Noble metal decoration on N-doped graphene and rGO: Noble metals such as Au [109], Pt [110], Pd [111], Ag [112], and Rh [113] are commonly used for the decoration of metal oxide gas sensors. They have catalytic activity towards some gases and can facilitate the adsorption and dissociation of gases on the surface of N-doped graphene. Furthermore, due to having a different work function than N-doped graphene or N-doped rGO, upon intimate contact, they will form heterojunctions with N-doped graphene or N-doped rGO with potential barriers to the flow of charge carriers. In the presence of target gases, due to related reactions and the release of abstraction of electrons on the sensor surface, the height of potential barriers changes, leading to a resistance modulation of the gas senor. In this way, it is expected that the overall response of the sensor will increase after noble metal decoration.

(iv) Investigation of the effect of high-energy irradiation on the sensing properties of N-doped graphene or rGO: Generally, high-energy ion beams such as electron beams [114], laser irradiation [115], and gamma rays [116] cause the breaking of bonds and the formation of structural defects within the regions near the surface of the host material. These formed defects are favorable sites for the adsorption of gases, and it is expected that more gases will be adsorbed on the sensor after high-energy irradiation. However, it should be noted that, generally, there is an optimal dosage of irradiation where the maximum response is observed [117]. Hence, the effect of high-energy irradiation on the response of N-doped graphene or N-doped rGO should be investigated.

(v) Hybrids of CPs with N-doped graphene for gas-sensing studies: Even though some works in this aspect have been reported, it seems that more studies are necessary. Generally, CPs such as graphene can work at low or room temperature, and some of them have a good sensing response to some gases such as NH_3 [118]. Hence, hybrids of CPs with N-doped graphene or N-doped rGO can enhance the overall sensing performance.

(vi) Hybrids of MXenes with N-doped graphene for gas-sensing studies: MXenes are a new family of 2D materials. They are synthesized via the etching of the MAX phase, and the resultant accordion-like morphology with open channels is very promising for the diffusion of gases [119]. Furthermore, they can work at low or room temperature [120]. Hence, hybrids of MXenes with N-doped graphene or N-doped rGO can work at room temperature; with a high surface area and good conductivity, all are beneficial for sensing applications.

References

1. Navale, S.; Mirzaei, A.; Majhi, S.M.; Kim, H.W.; Kim, S.S. State-of-the-art research on chemiresistive gas sensors in Korea: Emphasis on the achievements of the research labs of professors Hyoun Woo Kim and Sang Sub Kim. *Sensors* **2022**, *22*, 61. [CrossRef] [PubMed]
2. Navale, S.; Shahbaz, M.; Majhi, S.M.; Mirzaei, A.; Kim, H.W.; Kim, S.S. Cu_xO nanostructure-based gas sensors for H_2S detection: An overview. *Chemosensors* **2021**, *9*, 127. [CrossRef]
3. Mirzaei, A.; Ansari, H.R.; Shahbaz, M.; Kim, J.-Y.; Kim, H.W.; Kim, S.S. Metal Oxide Semiconductor Nanostructure Gas Sensors with Different Morphologies. *Chemosensors* **2022**, *10*, 289. [CrossRef]
4. Kotecha, A.M.; Corrêa, A.D.C.; Fisher, K.M.; Rushworth, J.V. Olfactory dysfunction as a global biomarker for sniffing out Alzheimer's disease: A meta-analysis. *Biosensors* **2018**, *8*, 41. [CrossRef]
5. Mirzaei, A.; Kim, S.S.; Kim, H.W. Resistance-based H_2S gas sensors using metal oxide nanostructures: A review of recent advances. *J. Hazard. Mater.* **2018**, *357*, 314–331. [CrossRef]
6. Majhi, S.M.; Mirzaei, A.; Kim, H.W.; Kim, S.S. Recent advances in energy-saving chemiresistive gas sensors: A review. *Nano Energy* **2021**, *79*, 105369. [CrossRef]
7. Chen, C.; Jiang, M.; Luo, X.; Tai, H.; Jiang, Y.; Yang, M.; Xie, G.; Su, Y. Ni-Co-P hollow nanobricks enabled humidity sensor for respiratory analysis and human-machine interfacing. *Sens. Actuators B Chem.* **2022**, *370*, 132441. [CrossRef]
8. Su, Y.; Liu, Y.; Li, W.; Xiao, X.; Chen, C.; Lu, H.; Yuan, Z.; Tai, H.; Jiang, Y.; Zou, J.; et al. Sensing-transducing coupled piezoelectric textiles for self-powered humidity detection and wearable biomonitoring. *Mater. Horiz.* **2023**, *10*, 842–851. [CrossRef]
9. Mirzaei, A.; Kordrostami, Z.; Shahbaz, M.; Kim, J.-Y.; Kim, H.W.; Kim, S.S. Resistive-Based Gas Sensors Using Quantum Dots: A Review. *Sensors* **2022**, *22*, 4369. [CrossRef]
10. Navale, S.; Shahbaz, M.; Mirzaei, A.; Kim, S.S.; Kim, H.W. Effect of Ag addition on the gas-sensing properties of nanostructured resistive-based gas sensors: An overview. *Sensors* **2021**, *21*, 6454. [CrossRef]
11. Brattain, W.H.; Bardeen, J. Surface properties of germanium. *Bell Syst. Tech. J.* **1953**, *32*, 1–41. [CrossRef]
12. Seiyama, T.; Kato, A.; Fujiishi, K.; Nagatani, M. A new detector for gaseous components using semiconductive thin films. *Anal. Chem.* **1962**, *34*, 1502–1503. [CrossRef]
13. Zhang, J.; Liu, X.; Neri, G.; Pinna, N. Nanostructured materials for room-temperature gas sensors. *Adv. Mater.* **2016**, *28*, 795–831. [CrossRef] [PubMed]
14. Wong, Y.C.; Ang, B.C.; Haseeb, A.S.M.A.; Baharuddin, A.A.; Wong, Y.H. Conducting polymers as chemiresistive gas sensing materials: A review. *J. Electrochem. Soc.* **2020**, *167*, 037503. [CrossRef]
15. Llobet, E. Gas sensors using carbon nanomaterials: A review. *Sens. Actuators B Chem.* **2013**, *179*, 32–45. [CrossRef]
16. Deshmukh, K.; Kovářík, T.; Pasha, S.K.K. State of the art recent progress in two dimensional MXenes based gas sensors and biosensors: A comprehensive review. *Coord. Chem. Rev.* **2020**, *424*, 213514. [CrossRef]
17. Kumar, R.; Goel, N.; Hojamberdiev, M.; Kumar, M. Transition metal dichalcogenides-based flexible gas sensors. *Sens. Actuators A Phys.* **2020**, *303*, 111875. [CrossRef]
18. Mirzaei, A.; Janghorban, K.; Hashemi, B.; Bonyani, M.; Leonardi, S.G.; Neri, G. A novel gas sensor based on Ag/Fe_2O_3 core-shell nanocomposites. *Ceram. Int.* **2016**, *42*, 18974–18982. [CrossRef]
19. Zhang, Y.; Zhang, Y.; Zhang, D.; Li, S.; Jiang, C.; Su, Y. Confinement preparation of Au nanoparticles embedded in ZIF-67-derived N-doped porous carbon for high-performance detection of hydrazine in liquid/gas phase. *Sens. Actuators B Chem.* **2019**, *285*, 607–616. [CrossRef]
20. Novoselov, K.S.; Geim, A.K.; Morozov, S.V.; Jiang, D.; Zhang, Y.; Dubonos, S.V.; Grigorieva, I.V.; Firsov, A.A. Electric field effect in atomically thin carbon films. *Science* **2004**, *306*, 666–669. [CrossRef]
21. Geim, A.K.; Novoselov, K.S. The rise of graphene. *Nat. Mater.* **2007**, *6*, 183–191. [CrossRef] [PubMed]
22. Razaq, A.; Bibi, F.; Zheng, X.; Papadakis, R.; Jafri, S.H.M.; Li, H. Review on graphene-, graphene oxide-, reduced graphene oxide-based flexible composites: From fabrication to applications. *Materials* **2022**, *15*, 1012. [CrossRef] [PubMed]
23. Kaur, R.; Arora, A.; Tripathi, S.K. Fabrication and characterization of metal insulator semiconductor Ag/PVA/GO/PVA/n-Si/Ag device. *Microelec. Eng.* **2020**, *233*, 111419. [CrossRef]
24. Ren, P.G.; Yan, D.X.; Ji, X.; Chen, T.; Li, Z.M. Temperature dependence of graphene oxide reduced by hydrazine hydrate. *Nanotechnology* **2010**, *22*, 055705. [CrossRef]
25. Majhi, S.M.; Mirzaei, A.; Kim, H.W.; Kim, S.S. Reduced graphene oxide (rGO)-loaded metal-oxide nanofiber gas sensors: An overview. *Sensors* **2021**, *21*, 1352. [CrossRef]
26. He, D.; Jiang, Y.; Lv, H.; Pan, M.; Mu, S. Nitrogen-doped reduced graphene oxide supports for noble metal catalysts with greatly enhanced activity and stability. *Appl. Catal. B Environ.* **2013**, *132*, 379–388. [CrossRef]
27. Luo, Z.; Lim, S.; Tian, Z.; Shang, J.; Lai, L.; MacDonald, B.; Fu, C.; Shen, Z.; Yu, T.; Lin, J. Pyridinic N doped graphene: Synthesis, electronic structure, and electrocatalytic property. *J. Mater. Chem.* **2011**, *21*, 8038–8044. [CrossRef]
28. Kazemi, A.; Rodner, M.; Fadavieslam, M.R.; Kaushik, P.D.; Ivanov, I.G.; Eriksson, J.; Syväjärvi, M.; Yakimova, R.; Yazdi, G.R. The effect of Cl- and N-doped MoS_2 and WS_2 coated on epitaxial graphene in gas-sensing applications. *Surf. Interfaces* **2021**, *25*, 101200. [CrossRef]
29. Varghese, S.S.; Lonkar, S.; Singh, K.K.; Swaminathan, S.; Abdala, A. Recent advances in graphene based gas sensors. *Sens. Actuators B Chem.* **2015**, *218*, 160–183. [CrossRef]

30. Sahu, D.; Sutar, H.; Senapati, P.; Murmu, R.; Roy, D. Graphene, graphene-derivatives and composites: Fundamentals, synthesis approaches to applications. *J. Compos. Sci.* **2021**, *5*, 181. [CrossRef]

31. Wang, C.-N.; Li, Y.-L.; Gong, F.-L.; Zhang, Y.-H.; Fang, S.-M.; Zhang, H.-L. Advances in doped ZnO nanostructures for gas sensor. *Chem. Rec.* **2020**, *20*, 1553–1567. [CrossRef] [PubMed]

32. Lv, R.; Terrones, M. Towards new graphene materials: Doped graphene sheets and nanoribbons. *Mater. Lett.* **2012**, *78*, 209–218. [CrossRef]

33. Putri, L.K.; Ong, W.j.; Chang, W.S.; Chai, S.P. Heteroatom doped graphene in photocatalysis: A review. *Appl. Surf. Sci.* **2015**, *358*, 2–14. [CrossRef]

34. Sui, Y.; Zhu, B.; Zhang, H.; Shu, H.; Chen, Z.; Zhang, Y.; Zhang, Y.; Wang, B.; Tang, C.; Xie, X.; et al. Temperature-dependent nitrogen configuration of N-doped graphene by chemical vapor deposition. *Carbon* **2015**, *81*, 814–820. [CrossRef]

35. Shao, L.; Chen, G.; Ye, H.; Wu, Y.; Qiao, Z.; Zhu, Y.; Niu, H. Sulfur dioxide adsorbed on graphene and heteroatom-doped graphene: A first-principles study. *Eur. Phys. J. B* **2013**, *86*, 54. [CrossRef]

36. Salih, E.; Ayesh, A.I. Sensitive SO_2 gas sensor utilizing Pt-doped graphene nanoribbon: First principles investigation. *Mater. Chem. Phys.* **2021**, *267*, 124695. [CrossRef]

37. Guo, B.; Fang, L.; Zhang, B.; Gong, J.R. Graphene doping: A review. *Insciences J.* **2011**, *1*, 80–89. [CrossRef]

38. Gaidukevic, J.; Aukstakojyte, R.; Kozłowski, M.; Barkauskas, J.; Pauliukaite, R. A Simple Preparation of N-doped Reduced Graphene Oxide as an Electrode Material for the Detection of Hydrogen Peroxide and Glucose. *Electrochim. Acta* **2023**, *446*, 142113. [CrossRef]

39. Zhang, Y.; Wu, L.; Lei, W.; Xia, X.; Xia, M.; Hao, Q. Electrochemical determination of 4-nitrophenol at polycarbazole/N-doped graphene modified glassy carbon electrode. *Electrochim. Acta* **2014**, *146*, 568–576. [CrossRef]

40. Fan, M.; Feng, Z.-Q.; Zhu, C.; Chen, X.; Chen, C.; Yang, J.; Sun, D. Recent progress in 2D or 3D N-doped graphene synthesis and the characterizations, properties, and modulations of N species. *J. Mater. Sci.* **2016**, *51*, 10323–10349. [CrossRef]

41. Lin, L.-Y.; Kavadiya, S.; Soundappan, T.; Biswas, P. N-doped reduced graphene oxide promoted nano TiO_2 as a bifunctional adsorbent/photocatalyst for CO_2 photoreduction: Effect of N species. *Chem. Eng. J.* **2017**, *316*, 449–460. [CrossRef]

42. Yang, S.; Li, G.; Wang, D.; Qiao, Z.; Qu, L. Synthesis of nanoneedle-like copper oxide on N-doped reduced graphene oxide: A three-dimensional hybrid for nonenzymatic glucose sensor. *Sens. Actuators B Chem.* **2017**, *238*, 588–595. [CrossRef]

43. Liu, P.; Zhang, Y.; Yan, J.; Huang, Y.; Xia, L.; Guang, Z. Synthesis of lightweight N-doped graphene foams with open reticular structure for high-efficiency electromagnetic wave absorption. *Chem. Eng. J.* **2019**, *368*, 285–298. [CrossRef]

44. Li, L.; Liu, D.; Wang, K.; Mao, H.; You, T. Quantitative detection of nitrite with N-doped graphene quantum dots decorated N-doped carbon nanofibers composite-based electrochemical sensor. *Sens. Actuators B Chem.* **2017**, *252*, 17–23. [CrossRef]

45. Janyasupab, M.; Liu, C.-W.; Chanlek, N.; Chio-Srichan, S.; Promptmas, C.; Surareungchai, W. A comparative study of non-enzymatic glucose detection in artificial human urine and human urine specimens by using mesoporous bimetallic cobalt-iron supported N-doped graphene biosensor based on differential pulse voltammetry. *Sens. Actuators B Chem.* **2019**, *286*, 550–563. [CrossRef]

46. Du, X.; Dai, L.; Jiang, D.; Li, H.; Hao, N.; You, T.; Mao, H.; Wang, K. Gold nanrods plasmon-enhanced photoelectrochemical aptasensing based on hematite/N-doped graphene films for ultrasensitive analysis of 17β-estradiol. *Biosens. Bioelectron.* **2017**, *91*, 706–713. [CrossRef]

47. Singh, S.K.; Tiwari, N.K.; Yadav, A.K.; Akhtar, M.J.; Kar, K.K. Design of ZnO/N-doped graphene nanohybrid incorporated RF complementary split ring resonator sensor for ammonia gas detection. *IEEE Sens. J.* **2019**, *19*, 7968–7975. [CrossRef]

48. Wu, S.; Deng, D.; Zhang, E.; Li, H.; Xu, L. CoN nanoparticles anchored on ultra-thin N-doped graphene as the oxygen reduction electrocatalyst for highly stable zinc-air batteries. *Carbon* **2022**, *196*, 347–353. [CrossRef]

49. Karatekin, R.S.; Kaplan, S.; Ozmen, S.I.; Dudukcu, M.K. N-doped reduced graphene oxide/ZnO/nano-Pt composites for hydrogen peroxide sensing. *Mater. Chem. Phys.* **2022**, *280*, 125792. [CrossRef]

50. Hadadian, M.; Correa-Baena, J.-P.; Goharshadi, E.K.; Ummadisingu, A.; Seo, J.-Y.; Luo, J.; Gholipour, S.; Zakeeruddin, S.M.; Saliba, M.; Abate, A.; et al. Enhancing efficiency of perovskite solar cells via N-doped graphene: Crystal modification and surface passivation. *Adv. Mater.* **2016**, *28*, 8681–8686. [CrossRef]

51. Xiong, C.; Li, M.; Zhao, W.; Duan, C.; Ni, Y. Flexible N-Doped reduced graphene oxide/carbon Nanotube-MnO_2 film as a Multifunctional Material for High-Performance supercapacitors, catalysts and sensors. *J. Mater.* **2020**, *6*, 523–531. [CrossRef]

52. Zhou, W.; Zhou, J.; Zhou, Y.; Lu, J.; Zhou, K.; Yang, L.; Tang, Z.; Li, L.; Chen, S. N-doped carbon-wrapped cobalt nanoparticles on N-doped graphene nanosheets for high-efficiency hydrogen production. *Chem. Mater.* **2015**, *27*, 2026–2032. [CrossRef]

53. Sardana, S.; Aggarwal, K.; Siwach, P.; Gaba, L.; Maan, A.S.; Singh, K.; Ohlan, A. Hierarchical three dimensional polyaniline/N-doped graphene nanocomposite hydrogel for energy storage applications. *Energy Storage* **2023**, *5*, e328. [CrossRef]

54. Wang, H.; Maiyalagan, T.; Wang, X. Review on recent progress in nitrogen-doped graphene: Synthesis, characterization, and its potential applications. *ACS Catal.* **2012**, *2*, 781–794. [CrossRef]

55. Vesel, A.; Zaplotnik, R.; Primc, G.; Mozetič, M. A review of strategies for the synthesis of N-doped graphene-like materials. *Nanomaterials* **2020**, *10*, 2286. [CrossRef] [PubMed]

56. Zhang, J.; Zhao, C.; Liu, N.; Zhang, H.; Liu, J.; Fu, Y.Q.; Guo, B.; Wang, Z.; Lei, S.; Hu, P. Tunable electronic properties of graphene through controlling bonding configurations of doped nitrogen atoms. *Sci. Rep.* **2016**, *6*, 28330. [CrossRef]

57. Schiros, T.; Nordlund, D.; Pálová, L.; Prezzi, D.; Zhao, L.; Kim, K.S.; Wurstbauer, U.; Gutiérrez, C.; Delongchamp, D.; Jaye, C.; et al. Connecting dopant bond type with electronic structure in N-doped graphene. *Nano Lett.* **2012**, *12*, 4025–4031. [CrossRef]

58. Bhuyan, M.S.A.; Uddin, M.N.; Islam, M.M.; Bipasha, F.A.; Hossain, S.S. Synthesis of graphene. *Int. Nano Lett.* **2016**, *6*, 65–83. [CrossRef]

59. Pham, T.V.; Kim, J.-G.; Jung, J.Y.; Kim, J.H.; Cho, H.; Seo, T.H.; Lee, H.; Kim, N.D.; Kim, M.J. High areal capacitance of N-doped graphene synthesized by arc discharge. *Adv. Funct. Mater.* **2019**, *29*, 1905511. [CrossRef]

60. Son, M.; Chee, S.-S.; Kim, S.-Y.; Lee, W.; Kim, Y.H.; Oh, B.-Y.; Hwang, J.Y.; Lee, B.H.; Ham, M.-H. High-quality nitrogen-doped graphene films synthesized from pyridine via two-step chemical vapor deposition. *Carbon* **2020**, *159*, 579–585. [CrossRef]

61. Liu, C.; Zhang, L.; Liu, R.; Gao, Z.; Yang, X.; Tu, Z.; Yang, F.; Ye, Z.; Cui, L.; Xu, C.; et al. Hydrothermal synthesis of N-doped TiO2 nanowires and N-doped graphene heterostructures with enhanced photocatalytic properties. *J. Alloys Compd.* **2016**, *656*, 24–32. [CrossRef]

62. Wang, D.-W.; Gentle, I.R.; Lu, G.Q. Enhanced electrochemical sensitivity of PtRh electrodes coated with nitrogen-doped graphene. *Electrochem. Commun.* **2010**, *12*, 1423–1427. [CrossRef]

63. Fouda, A.N.; Duraia, E.S.M.; Almaqwashi, A.A. Facile and scalable green synthesis of N-doped graphene/CNTs nanocomposites via ball milling. *Ain Shams Eng. J.* **2021**, *12*, 1017–1024. [CrossRef]

64. Magureanu, M.; Mandache, N.B.; Rizescu, C.; Bucur, C.; Cojocaru, B.; Man, I.C.; Primo, A.; Parvulescu, V.I.; Garcia, H. Engineering hydrogenation active sites on graphene oxide and N-doped graphene by plasma treatment. *Appl. Catal. B Environ.* **2021**, *287*, 119962. [CrossRef]

65. Lemes, G.; Sebastián, D.; Pastor, E.; Lázaro, M.J. N-doped graphene catalysts with high nitrogen concentration for the oxygen reduction reaction. *J. Power Sources* **2019**, *438*, 227036. [CrossRef]

66. Zhang, X.; Zhang, X.; Zhao, S.; Wang, Y.Q.; Lin, X.; Tian, Z.Q.; Shen, P.K.; Jiang, S.P. Precursor modulated active sites of nitrogen doped graphene-based carbon catalysts via one-step pyrolysis method for the enhanced oxygen reduction reaction. *Electrochim. Acta* **2021**, *370*, 137712. [CrossRef]

67. Kuniyil, M.; Kumar, J.V.S.; Adil, S.F.; Shaik, M.R.; Khan, M.; Assal, M.E.; Siddiqui, M.R.H.; Al-Warthan, A. One-pot synthesized Pd@N-doped graphene: An efficient catalyst for Suzuki–Miyaura couplings. *Catalysts* **2019**, *9*, 469. [CrossRef]

68. Deokar, G.; Jin, J.; Schwingenschlögl, U.; Costa, P.M.F.J. Chemical vapor deposition-grown nitrogen-doped graphene's synthesis, characterization and applications. *npj 2D Mater. Appl.* **2022**, *6*, 14. [CrossRef]

69. Wang, J.-B.; Ren, Z.; Hou, Y.; Yan, X.; Liu, P.; Zhang, H.; Zhang, H.; Guo, J. A review of graphene synthesis at low temperatures by CVD methods. *New Carbon Mater.* **2020**, *35*, 193–208. [CrossRef]

70. Yadav, R.; Dixit, C.K. Synthesis, characterization and prospective applications of nitrogen-doped graphene: A short review. *J. Sci. Adv. Mater. Dev.* **2017**, *2*, 141–149. [CrossRef]

71. Ikram, R.; Mohamed Jan, B.; Atif Pervez, S.; Papadakis, V.M.; Ahmad, W.; Bushra, R.; Kenanakis, G.; Rana, M. Recent advancements of N-doped graphene for rechargeable batteries: A review. *Crystals* **2020**, *10*, 1080. [CrossRef]

72. Xu, H.; Ma, L.; Jin, Z. Nitrogen-doped graphene: Synthesis, characterizations and energy applications. *J. Energy Chem.* **2018**, *27*, 146–160. [CrossRef]

73. Yan, Z.; Zhang, Y.; Kang, W.; Deng, N.; Pan, Y.; Sun, W.; Ni, J.; Kang, X. TiO2 Gas sensors combining experimental and DFT calculations: A review. *Nanomaterials* **2022**, *12*, 3611. [CrossRef] [PubMed]

74. Spencer, M.J. Gas sensing applications of 1D-nanostructured zinc oxide: Insights from density functional theory calculations. *Prog. Mater. Sci.* **2012**, *57*, 437–486. [CrossRef]

75. Cruz-Martínez, H.; Rojas-Chávez, H.; Montejo-Alvaro, F.; Peña-Castañeda, Y.A.; Matadamas-Ortiz, P.T.; Medina, D.I. Recent developments in graphene-based toxic gas sensors: A theoretical overview. *Sensors* **2021**, *21*, 1992. [CrossRef]

76. Ma, C.C.; Shao, X.H.; Cao, D.P. Nitrogen-doped graphene as an excellent candidate for selective gas sensing. *Sci. China Chem.* **2014**, *57*, 911–917. [CrossRef]

77. Wang, W.; Zhang, Y.; Shen, C.; Chai, Y. Adsorption of CO molecules on doped graphene: A first-principles study. *AIP Adv.* **2016**, *6*, 025317. [CrossRef]

78. Liu, X.-Y.; Zhang, J.-M. Formaldehyde molecule adsorbed on doped graphene: A first-principles study. *Appl. Surf. Sci.* **2014**, *293*, 216–219. [CrossRef]

79. Zheng, Z.; Wang, H. Different elements doped graphene sensor for CO2 greenhouse gases detection: The DFT study. *Chem. Phys. Lett.* **2019**, *721*, 33–37. [CrossRef]

80. Hamaya, N.; Ishizuka, M.; Onoda, S.; Guishan, J.; Ohmura, A.; Shimizu, K. Pressure-induced phase transition, metallization, and superconductivity in boron triiodide. *Phys. Rev. B* **2010**, *82*, 094506. [CrossRef]

81. Rad, A.S.; Shadravan, A.; Soleymani, A.A.; Motaghedi, N. Lewis acid-base surface interaction of some boron compounds with N-doped graphene; first principles study. *Curr. Appl. Phys.* **2015**, *15*, 1271–1277. [CrossRef]

82. Zhang, H.; Luo, X.; Lin, X.; Lu, X.; Leng, Y. Density functional theory calculations of hydrogen adsorption on Ti-, Zn-, Zr-, Al-, and N-doped and intrinsic graphene sheets. *Int. J. Hydrogen Energy* **2013**, *38*, 14269–14275. [CrossRef]

83. Zhang, H.; Luo, X.; Lin, X.; Lu, X.; Leng, Y.; Song, H. Density functional theory calculations on the adsorption of formaldehyde and other harmful gases on pure, Ti-doped, or N-doped graphene sheets. *Appl. Surf. Sci.* **2013**, *283*, 559–565. [CrossRef]

84. Wang, Y.; Chen, J.; Huang, X. Adsorption behavior of B-doped/N-doped graphene sheets toward NO2, NO and NH3 molecules: A first-principles study. *Phys. Status Solidi C* **2017**, *14*, 1600110. [CrossRef]

85. Abe, I.; Fukuhara, T.; Maruyama, J.; Tatsumoto, H.; Iwasaki, S. Preparation of carbonaceous adsorbents for removal of chloroform from drinking water. *Carbon* **2001**, *39*, 1069–1073. [CrossRef]

86. Tian, Y.L.; Ren, J.F.; Yue, W.W.; Chen, M.N.; Hu, G.C.; Yuan, X.B. Adsorption of chloroform on N-doped and Al-doped graphene: A first-principle study. *Chem. Phys. Lett.* **2017**, *685*, 344–348. [CrossRef]

87. Rad, A.S.; Esfahanian, M.; Maleki, S.; Gharati, G. Application of carbon nanostructures toward SO_2 and SO_3 adsorption: A comparison between pristine graphene and N-doped graphene by DFT calculations. *J. Sulfur Chem.* **2016**, *37*, 176–188. [CrossRef]

88. Zhang, H.; Luo, X.; Lin, X.; Zhang, Y.; Tang, P.; Lu, X.; Tang, Y. Band structure of graphene modulated by Ti or N dopants and applications in gas sensing. *J. Mol. Graph. Model.* **2015**, *61*, 224–230. [CrossRef]

89. Vinayan, B.P.; Sethupathi, K.; Ramaprabhu, S. Facile synthesis of triangular shaped palladium nanoparticles decorated nitrogen doped graphene and their catalytic study for renewable energy applications. *Int. J. Hydrogen Energy* **2013**, *38*, 2240–2250. [CrossRef]

90. Tang, Y.; Zhang, H.; Chen, W.; Li, Z.; Teng, D.; Dai, X. Modulating geometric, electronic, gas sensing and catalytic properties of single-atom Pd supported on divacancy and N-doped graphene sheets. *Appl. Surf. Sci.* **2020**, *508*, 145245. [CrossRef]

91. Carraro, G.; Celasco, E.; Smerieri, M.; Savio, L.; Bracco, G.; Rocca, M.; Vattuone, L. Chemisorption of CO on N-doped graphene on Ni (111). *Appl. Surf. Sci.* **2018**, *428*, 775–780. [CrossRef]

92. Kaur, M.; Kaur, M.; Sharma, V.K. Nitrogen-doped graphene and graphene quantum dots: A review on synthesis and applications in energy, sensors and environment. *Adv. Colloid Interface Sci.* **2018**, *259*, 44–64. [CrossRef] [PubMed]

93. Masemola, C.M.; Moloto, N.; Tetana, Z.N.; Gqoba, S.S.; Mubiayi, P.K.; Linganiso, E.C. N-doped graphene quantum dot-modified polyaniline for room-temperature sensing of alcohol vapors. *Mater. Chem. Phys.* **2022**, *287*, 126229. [CrossRef]

94. Kumar, V.; Mirzaei, A.; Bonyani, M.; Kim, K.-H.; Kim, H.W.; Kim, S.S. Advances in electrospun nanofiber fabrication for polyaniline (PANI)-based chemoresistive sensors for gaseous ammonia. *TrAC-Trends Anal. Chem.* **2020**, *129*, 115938. [CrossRef]

95. Gavgani, J.N.; Dehsari, H.S.; Hasani, A.; Mahyari, M.; Shalamzari, E.K.; Salehi, A.; Taromi, F.A. A room temperature volatile organic compound sensor with enhanced performance, fast response and recovery based on N-doped graphene quantum dots and poly(3,4-ethylenedioxythiophene)–poly(styrenesulfonate) nanocomposite. *RSC Adv.* **2015**, *5*, 57559–57567. [CrossRef]

96. Duan, K.; Li, W.; Zhu, C.; Li, J.; Xu, J.; Wang, X. Promoting sensitivity and selectivity of NO_2 gas sensor based on (P, N)-doped single-layer WSe_2: A first principles study. *Results Phys.* **2022**, *34*, 105296. [CrossRef]

97. Lv, Y.-K.; Li, Y.-Y.; Zhou, R.-H.; Pan, Y.-P.; Yao, H.-C.; Li, Z.-J. N-doped graphene quantum dot-decorated three-dimensional ordered macroporous In_2O_3 for NO_2 sensing at low temperatures. *ACS Appl. Mater. Interfaces* **2020**, *12*, 34245–34253. [CrossRef]

98. Chang, Y.-S.; Chen, F.-K.; Tsai, D.-C.; Kuo, B.-H.; Shieu, F.-S. N-doped reduced graphene oxide for room-temperature NO gas sensors. *Sci. Rep.* **2021**, *11*, 20719. [CrossRef]

99. Yan, W.-Y.; Zhou, Q.; Chen, X.; Huang, X.-J.; Wu, Y.-C. C-doped and N-doped reduced graphene oxide/TiO_2 composites with exposed (0 0 1) and (1 0 1) facets controllably synthesized by a hydrothermal route and their gas sensing characteristics. *Sens. Actuators B Chem.* **2016**, *230*, 761–772. [CrossRef]

100. Lin, G.; Wang, H.; Lai, X.; Yang, R.; Zou, Y.; Wan, J.; Liu, D.; Jiang, H.; Hu, Y. Co_3O_4/N-doped RGO nanocomposites derived from MOFs and their highly enhanced gas sensing performance. *Sens. Actuators B Chem.* **2020**, *303*, 127219. [CrossRef]

101. Modak, M.; Jagtap, S. Low temperature operated highly sensitive, selective and stable NO_2 gas sensors using N-doped SnO_2-rGO nanohybrids. *Ceram. Int.* **2022**, *48*, 19978–19989. [CrossRef]

102. Niu, F.; Liu, J.-M.; Wang, W.; Song, W.-G. Nitrogen and silica co-doped graphene nanosheets for NO_2 gas sensing. *J. Mater. Chem. A* **2013**, *1*, 6130–6133. [CrossRef]

103. Timmer, B.; Olthuis, W.; Van Den Berg, A. Ammonia sensors and their applications—A review. *Sens. Actuators B Chem.* **2005**, *107*, 666–677. [CrossRef]

104. Wu, Z.; Chen, X.; Zhu, S.; Zhou, Z.; Yao, Y.; Quan, W.; Liu, B. Enhanced sensitivity of ammonia sensor using graphene/polyaniline nanocomposite. *Sens. Actuators B Chem.* **2013**, *178*, 485–493. [CrossRef]

105. Gavgani, J.N.; Hasani, A.; Nouri, M.; Mahyari, M.; Salehi, A. Highly sensitive and flexible ammonia sensor based on S and N co-doped graphene quantum dots/polyaniline hybrid at room temperature. *Sens. Actuators B Chem.* **2016**, *229*, 239–248. [CrossRef]

106. Hakimi, M.; Salehi, A.; Boroumand, F.A.; Mosleh, N. Fabrication of a room temperature ammonia gas sensor based on polyaniline with N-doped graphene quantum dots. *IEEE Sens. J.* **2018**, *18*, 2245–2252. [CrossRef]

107. Hakimi, M.; Salehi, A.; Boroumand, F.A. Fabrication and characterization of an ammonia gas sensor based on PEDOT-PSS with N-doped graphene quantum dots dopant. *IEEE Sens. J.* **2016**, *16*, 6149–6154. [CrossRef]

108. Purbia, R.; Kwon, Y.M.; Kim, H.D.; Lee, Y.S.; Shin, H.; Baik, J.M. Zero-dimensional heterostructures: N-doped graphene dots/SnO_2 for ultrasensitive and selective NO_2 gas sensing at low temperatures. *J. Mater. Chem. A* **2020**, *8*, 11734–11742. [CrossRef]

109. Korotcenkov, G.; Brinzari, V.; Cho, B.K. Conductometric gas sensors based on metal oxides modified with gold nanoparticles: A review. *Microchim. Acta* **2016**, *183*, 1033–1054. [CrossRef]

110. Fu, X.; Yang, P.; Xiao, X.; Zhou, D.; Huang, R.; Zhang, X.; Cao, F.; Xiong, J.; Hu, Y.; Tu, Y.; et al. Ultra-fast and highly selective room-temperature formaldehyde gas sensing of Pt-decorated MoO_3 nanobelts. *J. Alloys Comp.* **2019**, *797*, 666–675. [CrossRef]

111. Mirzaei, A.; Yousefi, H.R.; Falsafi, F.; Bonyani, M.; Lee, J.H.; Kim, J.H.; Kim, H.W.; Kim, S.S. An overview on how Pd on resistive-based nanomaterial gas sensors can enhance response toward hydrogen gas. *Int. J. Hydrogen Energy* **2019**, *44*, 20552–20571. [CrossRef]

112. Yousefi, H.R.; Hashemi, B.; Mirzaei, A.; Roshan, H.; Sheikhi, M.H. Effect of Ag on the ZnO nanoparticles properties as an ethanol vapor sensor. *Mater. Sci. Semicond. Process.* **2020**, *117*, 105172. [CrossRef]

113. Adeli, B.; Espid, E.; Taghipour, F. Selective sensing performance of UV-activated ZnO nanowires decorated with Ir and Rh nanoparticles. *Mater. Sci. Eng. B* **2023**, *290*, 116307. [CrossRef]

114. Mirzaei, A.; Bang, J.H.; Choi, M.S.; Han, S.; Lee, H.Y.; Kim, S.S.; Kim, H.W. Changes in characteristics of Pt-functionalized RGO nanocomposites by electron beam irradiation for room temperature NO_2 sensing. *Ceram. Int.* **2020**, *46*, 21638–21646. [CrossRef]

115. Park, H.; Kim, J.H.; Shin, W.S.; Mirzaei, A.; Kim, Y.J.; Kim, S.S.; Halik, M.; Park, C. Facile strategy for advanced selectivity and sensitivity of SnO_2 nanowire-based gas sensor using chemical affinity and femtosecond laser irradiation. *Sens. Actuators B Chem.* **2022**, *372*, 132657. [CrossRef]

116. Wang, X.; Shi, Z.; Yao, S.; Liao, F.; Ding, J.; Shao, M. Gamma ray irradiated $AgFeO_2$ nanoparticles with enhanced gas sensor properties. *J. Solid State Chem.* **2014**, *219*, 228–231. [CrossRef]

117. Majhi, S.M.; Mirzaei, A.; Navale, S.; Kim, H.W.; Kim, S.S. Boosting the sensing properties of resistive-based gas sensors by irradiation techniques: A review. *Nanoscale* **2021**, *13*, 4728–4757. [CrossRef]

118. Liu, X.; Zheng, W.; Kumar, R.; Kumar, M.; Zhang, J. Conducting polymer-based nanostructures for gas sensors. *Coord. Chem. Rev.* **2022**, *462*, 214517. [CrossRef]

119. Zhan, X.; Si, C.; Zhou, J.; Sun, Z. MXene and MXene-based composites: Synthesis, properties and environment-related applications. *Nanoscale Horiz.* **2020**, *5*, 235–258. [CrossRef]

120. Li, Q.; Li, Y.; Zeng, W. Preparation and application of 2D MXene-based gas sensors: A review. *Chemosensors* **2021**, *9*, 225. [CrossRef]